Nature Communications

https://doi.org/10.1038/s41467-026-69662-z

Article in Press

Synthesis of 3-desoxycollinoketone B and its ability to reduce Alzheimer-associated misfolded proteins

Received: 24 February 2025

Accepted: 4 February 2026

Cite this article as: Heo, S., Cha, M., Zhung, W. *et al.* Synthesis of 3-desoxycollinoketone B and its ability to reduce Alzheimer-associated misfolded proteins. *Nat Commun* (2026). https://doi.org/10.1038/s41467-026-69662-z

Seongrok Heo, Minhae Cha, Wonho Zhung, JiMin Kim, Sirisuk Keereewan, Illhwan Cho, MinSeol Park, Wonbin Seo, Heewon Shin, Soljee Yoon, Suhyun Ye, Jae-Kyung Heo, Hayoung Hwang, Woo Youn Kim, YoungSoo Kim & Sunkyu Han

Synthesis of 3-desoxy-collinoketone B and its ability to reduce Alzheimer-associated misfolded proteins

Seongrok Heo,[1,†] Minhae Cha,[2,†] Wonho Zhung,[1,†] JiMin Kim,[2] Sirisuk Keereewan,[1] Illhwan Cho,[2] MinSeol Park,[2] Wonbin Seo,[2] Heewon Shin,[2] Soljee Yoon,[2] Suhyun Ye,[2] Jae-Kyung Heo[3], Hayoung Hwang[3], Woo Youn Kim,[1,*] YoungSoo Kim,[2,*] and Sunkyu Han[1,*]

[1]Department of Chemistry, Korea Advanced Institute of Science & Technology (KAIST), Daejeon 34141, Republic of Korea

[2]Department of Pharmacy and Yonsei Institute of Pharmaceutical Sciences, College of Pharmacy, Yonsei University, Incheon 21983, Republic of Korea

[3]New Drug Development Center, Daegu-Gyeongbuk Medical Innovation Foundation, Daegu, 41061, Republic of Korea

[†]These authors contributed equally to this work.

*Correspondence: sunkyu.han@kaist.ac.kr, y.kim@yonsei.ac.kr, wooyoun@kaist.ac.kr

Abstract

Collinolactone, featuring a 7/10/6 tricyclic core, has been proposed to be biosynthesized via a transannular [6+4] cycloaddition reaction. Besides its intriguing architecture, collinolactone holds pharmaceutical promises due to its ability to disrupt amyloid-β (Aβ) and tau aggregation, which are specifically found as disease culprits in the brains of Alzheimer's disease (AD) patients and are key targets in current drug discovery efforts. However, challenges associated with its acquisition from a natural source and limited pharmacokinetic properties have hampered its further studies. Herein, we report the design, synthesis, and evaluation of 3-desoxy-collinoketone B, a collinolactone derivative with improved pharmacokinetics for AD treatment. A stereoselective transannular [6+4] cycloaddition efficiently construct the tricyclic core, allowing its scalable synthesis. AI-assisted binding prediction and simulations not only indicate superior binding of 3-desoxy-collinoketone B to Aβ and tau aggregates than collinolactone, but also suggest a mechanistic basis for fibril destabilization. *In vitro* studies confirm its inhibition and dissociation of Aβ and tau fibrils, while *in vivo* experiments in AD mouse models show substantial amelioration of cognitive functions and Aβ/tau-associated pathology.

Introduction

Transannular [6+4] cycloaddition reaction is a rare yet intriguing transformation in natural product biosynthesis.[1] It has been identified as a key step in the (bio)synthesis of densely functionalized and stereochemically complex polycyclic secondary metabolites such as spinosyn,[2] heronamide,[1 3] and streptoseomycin,[4 5] In 1999, the Zeeck group reported the isolation of collinolactone (**1**), featuring an architecturally complex 7/10/6 tricyclic bislactone core, from *Streptomyces* sp. Gö 40/10 (Fig. 1a).[6 7] Recently, the Grond research team reported that collinolactone (**1**) is biosynthesized via type I polyketide synthase involving a presumed (formal) [6+4] cycloaddition reaction of the macrolactone intermediate and a Baeyer–Villiger oxidation of collinoketone (**2**, later to be renamed as collinoketone A, *vide infra*).[8] Notably, the absolute stereochemistry of collinolactone (**1**) was unambiguously assigned based on a single crystal X-ray diffraction (SCXRD) analysis of collazulene, the oxidative congener of collinolactone (**1**).[8 9] During the revision of this manuscript,[10] the research team led by Trauner and Houk reported the synthesis of collinoketones B (**3**) and C and showed that the originally isolated collinoketone by the Grond group is collinoketone B (**3**) and not collinoketone A (**2**).[11] Notably, collinoketone B (**3**) contains (*S*) configuration at the C5 position and bears a (*Z*, *Z*, *E*) cyclodecatriene core when compared to collinoketone A (**2**) which contains the (*R*) configuration at C5 and the (*Z*, *E*, *E*) cyclodecatriene core.

Alzheimer's disease (AD) is characterized by the accumulation of misfolded amyloid-β (Aβ) and tau, causing neurodegeneration and cognitive decline.[12 13] Treatments that are commonly given to AD patients were limited to symptomatic relief through cholinesterase inhibitors and N-methyl-D-aspartate receptor antagonists, which provide temporal cognitive benefits without disease-modifying functions. Lately, amyloid-clearing monoclonal antibody drugs have been approved for commercial use[14 15] with notable limitations: 1) antibodies are large biomolecules that cannot cross the cell membrane, preventing them from targeting intracellular tau aggregates; 2) biologics require complex manufacturing processes, leading to high costs and limited availability for patients; 3) severe side effects include brain swelling and microhemorrhages, and the cognitive benefits observed have often been marginal. 4) tauopathy remains problematic in the brain of AD patients[16 17 18]

Both Aβ plaques and tau tangles are key hallmarks of AD and established targets for drug development. Emerging evidence suggests that these proteins work together to drive the disease progression.[19] This explains the disappointing outcomes of anti-Aβ clinical trials and suggests that therapies focusing solely on one of these targets may have fundamental therapeutic limitations. Hence, the development of dual pharmacological clinical candidates that target both Aβ plaques

and tau tangles is highly desirable.[20] Small molecules hold significant potential due to their ability to effectively cross the blood-brain barrier (BBB), to target both extracellular and intracellular aggregates, and to be administered orally with lower production costs. In fact, small molecule-based dual inhibitors of Aβ and tau aggregation have been reported.[21 22 23] However, these studies focused on the inhibition of Aβ and tau aggregations and not necessarily on their clearance. Therefore, there is an urgent need to develop small-molecule therapeutics capable of targeting both extracellular Aβ plaques and intracellular tau tangles and reducing their aggregations.

Previously, we reported the discovery of rhizolutin (collinolactone), later to be revised to be identical to collinolactone (**1**),[8] from ginseng-rhizosperic *Strepomyces* sp. WON17.[24] Notably, it was found that the natural product dissociates both Aβ plaques and tau tangles *in vitro*. *In vivo* investigations with AD transgenic mice showed that the compound significantly dissociates hippocampal plaques.[24] However, scalable acquisition of the natural product from natural sources was challenging due to its low isolation yield (210 mg from 700 L culture of *Strepomyces* sp. WON17). Furthermore, the compound was not accessible to the cortical region of the brain.

To address these limitations of collinolactone (**1**), we initiated a synthetic program aimed at synthesizing 3-desoxycollinoketone (**8**) in this work. We hypothesized that the desoxy derivative of collinoketone B (**3**) would show enhanced BBB permeability due to its increased lipophilicity. Additionally, we anticipated that the 3-desroxy derivative would offer higher chemical stability, as collinoketone B (**3**) or its synthetic precursors may be susceptible to β-hydroxy elimination. From a synthetic standpoint, we envisioned that 3-desoxycollinoketone B (**8**) could serve as a precursor to both collinoketone (**3**) and collinolactone (**1**) through an α,β-unsaturation of the ketone group and a Baeyer–Villiger oxidation reaction.

For the synthesis of the desoxy derivative of collinoketone (**3**), we designed a modular strategy that utilizes three fragments **4**, **5**, and **6**. These fragments would be convergently assembled via Horner–Wordsworth–Emmons olefination, Suzuki–Miyaura cross-coupling reaction, and Yamaguchi macrolactonization reaction (Fig. 1b). We then envisioned a transannular [6+4] cycloaddition of the resulting macrolactone **7**. The stereochemical outcomes of the biosynthetic [6+4] cycloaddition reaction have been reported to be dictated enzymatically.[4] Hence, we wondered what would be the stereochemical outcome of the chemically driven [6+4] cycloaddition reaction of macrolactone **7**. Herein, we delineate the chemically-driven transannular [6+4] cycloaddition reaction of macrolactone **7** and discuss the stereochemical outcome of tricycle **8** along with its DFT calculation-based rationalization. We predict the binding free energy of tricycle **8** to Aβ and tau aggregates via AI-assisted molecular modeling. Additionally, molecular dynamics simulation suggests a fibril dissociation mechanism whereby tricycle **8** binding disrupts

key interactions that stabilize the aggregate. Furthermore, we show that the resulting 3-desoxy derivative of collinoketone (**3**) reduces aggregation of both Aβ and tau *in vitro* and ameliorates learning and memory impairments *in vivo* (Fig. 1b).

Results and Discussion

Synthesis of the modules

Our synthesis commenced with the preparation of module 1 (**11**). Alkyne **9** was subjected to hydrozirconation and iodination to produce vinyl iodide **10** in 75% yield.[25] The resulting vinyl iodide **10** was then allowed to react with lithiated dimethyl methylphosphonate to yield phosphonate **11** in 72% yield (Fig. 2a).[26] For the synthesis of module 2 (**14**), epoxide **12** was reacted with isobutenylmagnesium bromide in the presence of CuI to afford the homoallylic alcohol compound.[27] The alcohol moiety of the resulting product was subsequently silylated to give compound **13** (92% yield over 2 steps, Fig. 2b). When compound **13** was allowed to react with SeO_2 in a refluxing ethanol solution, aldehyde **14** was obtained as a result of a selective allylic oxidation reaction in 62% yield.[28]

The synthesis of module 3 (**19**) commenced with a zirconium-catalyzed carboalumination of propargyl alcohol (**15**). The resulting methylated aluminum intermediate was subsequently allowed to react with iodine to afford vinyl iodide **16** in 58% yield (Fig. 2c).[29] The resulting alcohol **16** was then oxidized to aldehyde **17** in the presence of manganese oxide. When aldehyde **17** was reacted with (*tert*-butoxycarbonylmethylene)triphenylphosphorane, unsaturated ester **18** was formed via a Wittig reaction in 83% yield from alcohol **16**.[30] Treatment of vinyl iodide **18** with *n*-BuLi resulted in the formation of vinyl lithium intermediate which was subsequently allowed to react with $B(O^iPr)_3$. The resulting boronic ester was subsequently reacted with 3,4-diethylhexane-3,4-diol (the tetraethyl analogue of pinacol) to produce module 3 (**19**) in 85% yield.[31] It is important to note that vinyl iodide **18** and boronic ester **19** were kept in the dark to prevent light-mediated decompositions. Notably, all transformations involved in the synthesis of modules 1–3 (**11**–**19**) were performed on a >5g scale.

Assembly of the modules and biosynthetically inspired [6+4] cycloaddition reaction

With modules 1–3 (**11**–**19**) in hand, we proceeded with their assembly for the synthesis of macrolactone **7**, the key precursor for the transannular [6+4] cycloaddition reaction. Modules 1 (**11**) and 2 (**14**) were conjugated via a Horner–Wadsworth–Emmons (HWE) olefination reaction in the presence of barium hydroxide to produce unsaturated ketone **20**.[32 33] Vinyl iodide **20** was then conjugated with module 3 (**19**) via a Suzuki-Miyaura cross-coupling reaction in the presence of $Pd(PPh_3)_4$, silver oxide, and triphenyl arsine.[34] While the pinacol boronic acid group is commonly used in Suzuki–Miyaura cross-coupling reactions, we utilized the tetraethyl analog of pinacol-based boronic acid for the following reasons: (1) greater chemical stability and easier

purification of **19** by flash column chromatography compared to its pinacol boronic ester counterpart; and (2) a superior yield when using **19**.[35]

The TBS protecting group in **21** was chemoselectively removed upon the reaction of **21** with camphorsulfonic acid in methanol to forge alcohol **22** in 60% over 2 steps.[36] A 4:1 dichloromethane and TFA co-solvent was employed for the deprotection of the *tert*-butyl ester moiety. The resulting carboxylic acid derivative was reacted with 2,4,6-trichlorobenzoyl chloride and triethylamine for the formation of the anhydride intermediate, which was subsequently reacted with DMAP to yield macrolactone **7** in 60% yield over 2 steps (Fig. 3).[37]

With robust synthetic access to macrolactone **7**, the stage was set for the key transannular [6+4] cycloaddition reaction. Interestingly, when a toluene solution of lactone **7** was heated in the microwave at 200 °C, 3-desoxy-collinoketone B (**8a**) was obtained in 63% yield (Fig. 3). The relative stereochemistry of the compound was assigned based on meticulous NOE-based analyses. While 5-H, 18-H, 14-H, and 16-H are positioned on the top face of the tricyclic framework, 10-H, 12-H, 17-H, and 19-H are positioned on the bottom face of the molecule (Fig. 3). Furthermore, SCXRD analysis of compound **8a** unambiguously confirmed its structure. The observed (*S*)-configuration at the C5 position of **8a** and the *Z*-configuration at the C6–C7 olefin are noteworthy, as they are the opposite of that found in collinoketone A (**3**). 3-desoxy-collinoketone B (**8a**) was the only observed product under other attempted cycloaddition conditions.

To rationalize the observed stereochemical outcomes, we performed DFT calculations on the thermal [6+4] cycloaddition reaction of macrolactone **7**. The conformational constraints imposed by five alkene groups, including two tri-substituted olefins, a ketone, and an ester moiety induced a conformational bias in macrolactone **7**. This led to the adoption of two distinct conformers **7A** and **7B**. Conformer **7A** was calculated to undergo a [6+4] cycloaddition reaction to produce 3-desoxy-collinoketone B (**8a**) via **7A-TS**. On the other hand, conformer **7B** was calculated to yield *anti*-3-desoxy-collinoketone B (*anti*-**8b)**, with the C18-methyl group placed above and C19-methyl group located below the hypothetical plane formed by the 10-membered ring, via **7B-TS**. To identify lower-energy conformations of TS structures, we employed the CREST algorithm [38] in conjunction with the autoCG package developed by Lee et al.,[39] which facilitates the generation of appropriate input geometries for TS search methods. *Syn*-**8b**, the rotamer of *anti*-**8b** with both C18- and C19-methyl groups located above the hypothetical plane (the analogous conformer observed in naturally occurring collinolactone (**1**)),[9] was calculated to be 2.81 kcal/mol less stable than *anti*-**8b**. Importantly, 3-desoxy-collinoketone B (**8a**) was

calculated to be 9.65 kcal/mol more stable than 3-desoxycollinoketone B (**8b**). While 3-desoxy-collinoketone B (**8a**) adopts a *trans*-decalin-like structure with the fused cyclohexanone moiety in a stable chair conformation, the *cis*-fused six-membered ring in 3-desoxy-collinoketone B (**8b**) adopts a twisted-boat conformation with higher torsional strain, leading to a less stable structure (Fig. 4).

AI-assisted molecular modeling and simulation to assess the role of 3-desoxy-collinoketone B(8a) on $A\beta_{42}$ and Tau aggregates

Conceiving that 3-desoxy-collinoketone B (**8a**) and collinolactone (**1**) share an analogous molecular framework and collinolactone (**1**) has previously been reported to dissociate both $A\beta_{42}$ and Tau aggregates,[24] we speculated the potential of 3-desoxy-collinoketone B (**8a**) as an agent targeting both $A\beta_{42}$ and Tau. Focusing on the point that abnormal aggregation of $A\beta_{42}$ and Tau precedes the clinical symptoms of AD,[40] we investigated the role of 3-desoxy-collinoketone B(**8a**) in $A\beta_{42}$ and Tau binding and disaggregation, respectively, via AI-assisted molecular modeling and simulation.

We employed AI models and domain tools to model and assess binding structures, and run binding simulations of $A\beta_{42}$ and Tau aggregates (Fig. 5a). For model inputs, geometrically optimized molecular structure of each compound with M06-2X/6-31G(d,p) level theory was used, while experimental structures retrieved from RCSB[41] for $A\beta_{42}$ (PDB ID: 2BEG, 17-42 fragment) [42] and Tau (PDB ID: 5O3L, 306-378 fragment)[43] fibrils were used. First of all, binding poses between the compounds and fibrils were sampled with DiffDock-L[44 45], the state-of-the-art diffusion-based pose prediction model. While experimental validation remains the definite standard, the reliability of AI predictions can be enhanced through statistical robustness achieved by an ensemble across a sufficiently large number of samples.[46] In this light, 1,000 poses were sampled with DiffDock-L followed by energy relaxation with Smina[47], a fork of AutoDock Vina.[48] Unfavorable poses with weak Smina-predicted binding free energies were filtered out. (Supplementary Fig. 4a, 4c) Remaining poses are clustered based on root-mean-square deviations (RMSD) to obtain the set of the most probable binding poses. (Supplementary Fig. 4b, 4d) Details of the experimental settings related to the filtering and clustering are provided in the Supplementary Information.

Figs. 5b and **5d** show representative poses of 3-desoxy-collinoketone B (**8a**) bound to $A\beta_{42}$ and Tau, respectively, which serves as the cluster centers for each set. The non-covalent interactions between 3-desoxy-collinoketone B (**8a**) and each fibril were analyzed with protein-

ligand interaction profiler (PLIP)[49 50] (Figs. 5c, 5e). Analysis indicates that 3-desoxy-collinoketone B(**8a**) interacts with the $A\beta_{42}$ fibril by forming hydrophobic interactions with Phe19, Ala21, and Val36, and the oxygen of the ketone moiety forms a hydrogen bond with Ala21 (Fig. 5c). With the Tau fibril, 3-desoxy-collinoketone B(**8a**) forms hydrophobic interactions with Ile360 and His362 of multiple chains (Fig. 5e). The ketone moiety forms a hydrogen bond with Lys353, and the lactone moiety forms salt bridges with His362 of multiple chains.

Smina-predicted binding free energies of compounds 3-desoxy-collinoketone B (**8a**) and collinolactone (**1**) were compared across modeled binding poses on $A\beta_{42}$ and Tau fibrils. Stronger binding is hypothesized to correlate with a greater ability to disrupt intrinsic fibril interactions, thereby promoting disaggregation. The bar plots show the result (Fig. 5f), where 3-desoxy-collinoketone B(**8a**) binds strongly to both $A\beta_{42}$ ($P < 0.001$) and Tau ($P < 0.0001$) fibrils than collinolactone (**1**). This suggests that, despite variability in the sampled binding poses, 3-desoxy-collinoketone B(**8a**) steadily adopts favorable conformations that enable strong interactions with both fibrils.

To further support the credibility of our AI-based binding pose predictions, we additionally employed NeuralPLexer2[51]. Unlike DiffDock-L, which assumes a rigid protein structure, NeuralPLexer2 accounts for protein flexibility by modeling ligand binding in the context of an experimental protein template. We followed the same modeling protocol as used with DiffDock-L, except for the clustering step, which was omitted because no single reference fibril structure is available for calculating ligand RMSD. **Fig. 5g** illustrates the corresponding result, where 3-desoxy -collinoketone B (**8a**) consistently shows stronger binding on both $A\beta_{42}$ ($P < 0.01$) and Tau ($P < 0.0001$) fibrils. By presenting a similar tendency from two independent AI models, we conclude that 3-desoxy -collinoketone B (**8a**) interacts favorably with both fibrils.

To investigate the potential disaggregation effect of 3-desoxy -collinoketone B (**8a**), we performed 100 ns molecular dynamics (MD) simulations starting from the modeled binding structures (Figs. 5b, 5d). The full simulation details are provided in the Supplementary Information. **Fig. 5h** presents the Cα root-mean-square fluctuation (RMSF) profiles of the $A\beta_{42}$ fibril in the presence and absence of 3-desoxy -collinoketone B (**8a**). Notably, in the 3-desoxy -collinoketone B (**8a**)-bound system, increased flexibility is observed—particularly in residues 40-42 of the chains that 3-desoxy collinoketone B (**8a**) directly interacts with. Further analysis of the trajectories reveals that the backbone RMSD of the $A\beta_{42}$ fibril increases upon 3-desoxy -collinoketone B (**8a**) binding, the average number of intrafibrillar hydrogen bonds decreases from

42.5 to 39.3, indicating that the initial fibril structure becomes destabilized in the presence of the compound. (Supplementary Figs. 5a, 5b) **Fig. 5i** visually illustrates the progressive disruption of the $A\beta_{42}$ fibril upon the binding of 3-desoxy -collinoketone B (**8a**), as observed over the course of the 100 ns simulation. Simulation results for Tau fibrils are presented in Supplementary Figs. 5c–e. In the case of 3-desoxy-collinoketone B (**8a**) binding, both the backbone RMSD and residue-level RMSF increase, while the number of intrafibrillar hydrogen bonds remains largely unchanged.

Finally, we analyzed the non-covalent interaction patterns throughout the MD simulation using ProLIF,[52] to characterize the interactions between 3-desoxy -collinoketone B (**8a**) and the fibrils. Supplementary Fig. 6 and 7 illustrate the full interaction profiles of $A\beta_{42}$ and Tau, respectively. In the case of $A\beta_{42}$, our observation reveals persistent interactions between 3-desoxy -collinoketone B (**8a**) and Phe19, as well as Ile32, which are the residues located within the hydrophobic core region known to be essential for fibril formation.[53] [54] Disrupting the hydrophobic interaction within this region may promote amyloid destabilization. Beyond hydrophobic interactions, 3-desoxy-collinoketone B (**8a**) disrupts the inter-chain Asp23–Lys28 salt bridge between chain A and chain B (Supplementary Fig. 6). Without the ligand, the polar contact between Oδ of Asp23 and Nξ of Lys28 persists for approximately 21% of the simulation trajectory; however, this contact is completely lost when 3-desoxy collinoketone B (**8a**) is bound. While the interaction profile (Supplementary Fig. 6) indicates that Asp23 of chain A is integrally involved in hydrophobic interactions with 3-desoxy -collinoketone B (**8a**), we propose that such disruption of the inter-chain Asp23–Lys28 salt bridge represents one of the mechanisms by which 3-desoxy -collinoketone B (**8a**) destabilizes the protofilament structure. For Tau, we observed interactions involving Ile360 and His362, which were previously implicated in ligand binding in a recent crystallographic study.[55] However, the specific role of these residues in Tau aggregation remains unclear and warrants further investigation.

To gain experimental data regarding the binding of 3-desoxy-collinoketone B(**8a**) to $A\beta_{42}$ aggregates, the compound was incubated with FITC labeled-$A\beta_{42}$ on plates immobilized with $A\beta_{42}$ fragment hexamers to identify the inhibitory site. The result indicates that 3-desoxy-collinoketone B(**8a**) interacts with the $A\beta_{14\text{-}20}$ region (^{14}HQKLVFF^{20}), the hydrophobic core critical for Aβ aggregation (Supplementary Fig 17). This result was consistent with the MD simulation based on the AI-predicted structure. 3-desoxy-collinoketone B(**8a**) interacts with the $A\beta_{14–20}$ region, particularly through hydrophobic interactions with Phe19 (Supplementary Fig. 6). These findings

collectively suggest that 3-desoxy-collinoketone B(**8a**) targets the hydrophobic core of $A\beta_{42}$, thereby interfering with the key intermolecular interactions required for fibril formation.

Inhibitory and dissociative effects of 3-desoxy-collinoketone B (8a) against $A\beta_{42}$

We next assessed the properties of 3-desoxy-collinoketone B (**8a**) on AD-related proteins, $A\beta_{42}$ and Tau. First, we investigated the properties of 3-desoxy-collinoketone B (**8a**) against $A\beta_{42}$ fibrillation utilizing thioflavin-T (ThT), a fluorescent chemical that intercalates into the β-sheet structure of fibrils, thereby enabling the quantification of fibril formation.[56] A substantial increase in red-shifted ThT fluorescence intensity indicates enhanced fibril production. To assess the aggregation inhibitory efficacy, 3-desoxy-collinoketone B (**8a**) was incubated with $A\beta_{42}$ (20 μM) for 24 h at 37 °C, and ThT fluorescence intensity was measured post-incubation. The data was normalized to the ThT fluorescence intensity of the control, which consisted of $A\beta_{42}$ incubated without 3-desoxy-collinoketone B (**8a**) for 24 h. In a 2-fold serial dilution ranging from 1.95 μM to 1000 μM, 3-desoxy-collinoketone B (**8a**) significantly inhibited $A\beta_{42}$ fibril formation, reducing fibril levels by 23.97% ($P < 0.0001$) at the highest concentration compared to the untreated control (Fig. 6a). Subsequently, $A\beta_{42}$ was incubated for 24 h at 37 °C to obtain preaggregated fibrils to evaluate the ability of 3-desoxy-collinoketone B (**8a**) to dissociate $A\beta_{42}$ fibrils. The pre-aggregated $A\beta_{42}$ fibrils (20 μM) were then treated with 3-desoxy-collinoketone B (**8a**) in a 2-fold serial diluted for an additional 24 h at 37 °C. Treatment with 3-desoxy-collinoketone B (**8a**) led to significant dissociation of fibrillar aggregates, reducing fibril levels by 35.75% ($P < 0.0001$) at the highest concentration compared to the untreated control (Fig. 6b). These findings indicate that 3-desoxy-collinoketone B (**8a**) effectively inhibits $A\beta_{42}$ aggregation and dissociates pre-formed $A\beta_{42}$ fibrils.

Given that oligomeric $A\beta_{42}$ species are more strongly associated with neurotoxicity and cognitive dysfunction than $A\beta_{42}$ fibrils,[57] we further investigated whether 3-desoxy-collinoketone B (**8a**) could also dissociate $A\beta_{42}$ oligomers by conducting a plate-based amyloid aggregate assay. Since ThT primarily detects the β-sheet structure of fibrils, we utilized the amyloid aggregate assay (A3) with fluorescently labeled $A\beta_{42}$ to specifically observe oligomeric forms through fluorescence intensity. A 96-well microplate was prepared by utilizing immobilized $A\beta_{42}$ via thiol-maleimide conjugation, as previously reported.[58] Fluorescently labeled Flamma552-$A\beta_{42}$ was then incubated in each well for 8 h to induce the formation of oligomeric aggregates between the immobilized-$A\beta_{42}$ and the fluorescent-labeled Flamma552-$A\beta_{42}$ (Fig. 6c). Following incubation, the fluorescence intensities of the immobilized $A\beta_{42}$-flamma552-$A\beta_{42}$ complexes were measured to establish baseline values for individual wells. 3-desoxy-collinoketone B (**8a**) was subsequently added to the immobilized $A\beta_{42}$-flamma552-$A\beta_{42}$ complexes and incubated for an additional 24 h

to assess the dissociative efficacy of 3-desoxy-collinoketone B (**8a**) against $A\beta_{42}$ oligomers. The reduction in fluorescence intensity compared to the baseline was used to determine the extent of $A\beta_{42}$ oligomer dissociation. This experiment revealed that 3-desoxy-collinoketone B (**8a**) dissociated $A\beta_{42}$ oligomer composed of immobilized $A\beta_{42}$-flamma552-$A\beta_{42}$ complex by 51.50% ($P < 0.0001$), compared to the fluorescence intensity prior to 3-desoxy-collinoketone B (**8a**) treatment (Fig. 6c).

To evaluate the therapeutic efficacy of 3-desoxy-collinoketone B (**8a**) *in vivo*, we employed 5XFAD transgenic mice carrying amyloid precursor protein (APP) and presenilin 1 (PSEN1) mutations. 3-desoxy-collinoketone B (**8a**) exhibited high BBB permeability (P_e = 4.71e^{-6} cm/s), comparable to the highly permeable control, promazine hydrochloride (Fig. 6d). In a short-term study, 30 mg/kg/day of 3-desoxy-collinoketone B (**8a**) or vehicle (10% DMSO, 10% Tween80 in PBS) were administered to 5XFAD mice (n = 3/group) by daily oral gavage for five days. Following the administration period, all mice were sacrificed, and their brains were extracted to analyze the amounts of Aβ through chemical fluorescence staining and immunoblotting. Aβ plaques in the brain of mice were visualized by Thioflavin S (ThS) staining which appeared as small green dots in Fig. 6e.

The number of Aβ plaques in the mice brain was quantified, showing a reduction of 25.29% ($P = 0.0957$) in the cortex region and statistically significant reduction of 18.86% ($P = 0.0273$) in the hippocampal region of the 3-desoxy-collinoketone B (**8a**)-administered 5XFAD mice brain compared to the untreated 5XFAD mice brain (Figs. 6f, 6h). In order to quantify the concentrations of total Aβ and oligomeric Aβ in RIPA-soluble fractions, dot blot assays using 6E10 (anti-Aβ, detecting all Aβ forms) and A11 (anti-oligomer, detecting oligomeric Aβ) antibodies were performed. Intriguingly, we observed a significant decrease in total soluble Aβ concentrations in both cortical (27.43%, $P = 0.0482$) and hippocampal (18.70%, $P = 0.0439$) regions of 3-desoxy-collinoketone B (**8a**)-treated 5XFAD mice brain lysates compared to vehicle-treated 5XFAD mice brain lysates (Figs. 6g, 6i). A slight decrease in Aβ oligomer concentration was observed in both cortex (7.60%, $P = 0.2959$) and hippocampus (3.21%, $P = 0.5008$); however, this reduction did not extend to statistical significance. These findings indicate that 3-desoxy-collinoketone B (**8a**) possesses both Aβ aggregation inhibition and disaggregation mechanisms, thereby having the potential to clear Aβ plaques in an AD mouse brain.

Given that consistent brain exposure to 3-desoxy-collinoketone B (**8a**) through five-day consecutive administration resulted in the reduction of both Aβ plaque burden and soluble Aβ aggregates in 6.5-month-old 5XFAD mice brain, an age at which Aβ plaque formation is highly active, we sought to further clarify the mechanism of action. Specifically, we aimed to elucidate

whether the observed decrease in plaque burden was a direct consequence of plaque clearance or an indirect result of reducing soluble Aβ aggregates. We conducted additional experiments utilizing 8.0-month-old male 5XFAD transgenic mice characterized by an extensive plaque burden. Mice received 3-desoxy -collinoketone B (**8a**) (30 mg/kg/day) or vehicle three times per week for one month (n = 4/group), and age-matched wild-type mice (n = 8) were treated identically for long-term dosing *in vivo* toxicity evaluation. Throughout the dosing period, 3-desoxy -collinoketone B (**8a**) (30 mg/kg/day) treated mice exhibited no changes in body weight, feed intake, or behavior, and no mortality was observed (Supplementary Fig 13). ThS staining was performed to visualize Aβ plaques in the brain (Fig. 6j) and revealed a moderate reduction in Aβ plaque numbers in 3-desoxy -collinoketone B (**8a**)-administered 5XFAD mice brain (12.75% in cortex, $P = 0.2292$; 11.25% in hippocampus, $P = 0.2102$) (Figs. 6k, 6m). Dot blot assays on RIPA-soluble brain lysates showed significant decrease in cortical total soluble Aβ (49.69%, $P < 0.0001$) and soluble oligomeric Aβ (22.99%, $P = 0.0003$) (Fig. 6l), with modest non-significant reductions in hippocampus (total soluble Aβ aggregates: 23.64%, $P = 0.0583$; soluble oligomeric Aβ: 17.26%, $P = 0.1835$) (Fig. 6n).

To determine whether the reduction of soluble Aβ levels in 5XFAD mice was mediated by modulation of Aβ aggregates amount or by alterations in APP processing, we performed western blot analyses on RIPA-soluble cortex and hippocampus lysates. The expression level of APP remained unchanged in 3-desoxy -collinoketone B (**8a**)-treated mice compared with the untreated group (Supplementary Fig 12), indicating that 3-desoxy -collinoketone B (**8a**) effects on Aβ aggregates independent of APP processing. In addition, 3-desoxy -collinoketone B (**8a**) treatment reduced the expression level of ionized calcium-binding adapter molecule 1 (Iba-1), a marker of microglial activation, in the hippocampus (22.68%, $P = 0.001$), while cortical Iba-1 and glial fibrillary acidic protein (GFAP) levels remained unchanged (Supplementary Fig 12).

Inhibitory and dissociative effects of 3-desoxy-collinoketone B (8a) against tau and tau repeat domain 3

To explore the dual-targeting therapeutic potential of 3-desoxy-collinoketone B (**8a**) against both Aβ and tau, we conducted a ThT assay to evaluate its effect on tau aggregation, as the formation of paired helical filaments (PHFs) is also driven by β-sheet fibrillation.[59 60] We first examined the inhibitory efficacy of 3-desoxy-collinoketone B (**8a**) against tau K18, a recombinant fragment of tau that comprises the microtubule-binding domain, a critical region for driving tau PHF formation (Fig. 7a).[61] Tau K18 (35 μM) was incubated with 3-desoxy-collinoketone B (**8a**) for 3 days at 37 °C, and tau K18 fibril formation detected by ThT was normalized to the fluorescence

intensity of tau K18 incubated without 3-desoxy-collinoketone B (**8a**) for 3 days. Interestingly, treatment of 3-desoxy-collinoketone B (**8a**) significantly inhibited tau K18 fibril formation by 68.87% (P < 0.0001, Fig. 7b). To assess the dissociation efficacy of 3-desoxy-collinoketone B (**8a**), preaggregated tau K18 fibrils were generated by incubating tau K18 at 37 °C for 3 days. 3-desoxy-collinoketone B (**8a**) was subsequently co-incubated with the 3-day preaggregated tau K18 for an additional 3 days. ThT assay revealed that 3-desoxy-collinoketone B (**8a**) significantly reduced tau K18 fibrils by 50.85% (P < 0.0001) compared to the untreated control incubated for the same total duration (Fig. 7c). Additionally, compared to the 3-day preaggregated control before 3-desoxy-collinoketone B (**8a**) treatment, the tau K18 fibril was reduced by 41.36% (Fig. 7c). These results indicate that 3-desoxy-collinoketone B (**8a**) inhibits tau K18 aggregation and dissociates preaggregated tau K18.

Growing evidence indicates that Aβ plaques are closely associated with the initiation of AD pathology, which subsequently accelerates the formation of PHFs.[62 63] These PHFs contribute to neurofibrillary tangles (NFTs) and are strongly correlated with cognitive decline.[64 65] Therefore, the PS19 transgenic mouse model, carrying a mutation in MAPT P301S, was used to validate the therapeutic effect of 3-desoxy-collinoketone B (**8a**) on cognitive deficit by clearing PHFs *in vivo*. 3-desoxy-collinoketone B (**8a**) was administered orally at a dose of 30 mg/kg for 3 weeks to 6.5-month-old female PS19 mice. The control group, including wild-type and PS19 mice, was administered the vehicle (10% DMSO, 10% Tween 80 in PBS). After the 3-week administration period, all mice were sacrificed for immunoblot analysis. Increased tauopathy is associated with synaptic dysfunction, and both the postsynaptic marker postsynaptic density protein 95 (PSD95) and the presynaptic marker synaptophysin are reported to be downregulated in the presence of aggregated tau proteins.[66 67] To ascertain whether the 3-desoxy-collinoketone B (**8a**) administration could mitigate synaptic loss in the hippocampus, we evaluated the expression level of PSD95 and synaptophysin. The results demonstrated that the 3-desoxy-collinoketone B (**8a**) administration increased the expression levels of both PSD95 (7.60%, P = 0.0954) and synaptophysin (10.41%, P < 0.05) in the hippocampal region compared to the vehicle-treated PS19 mice (Fig. 7d).

The microtubule-binding domain of tau K18 comprises four tau repeat domains-R1, R2, R3, and R4-as dcted (Fig. 7a). Notably, tau filaments isolated from the brains of AD patients and individuals with other tauopathies exhibit a structured core primarily composed of tau repeat domains.[68] Additionally, increasing evidence suggests that repeat domain 3 (R3) is involved in neural system dysfunction, serving as a critical region for self-assembly and particularly associated with toxic effects.[69 70] Therefore, we estimated an inhibitory effect of 3-desoxy-

collinoketone B (**8a**) on R3 aggregation. R3 (35 μM) was incubated with or without 3-desoxy-collinoketone B (**8a**) in phosphate buffer saline (PBS) for 3 days at 37 °C. Co-incubation of R3 with 3-desoxy-collinoketone B (**8a**) significantly inhibited the formation of ThT-detected R3 fibrils by 88.18% ($P < 0.0001$, Fig. 7e). For the dissociation assay, R3 was preaggregated by incubating at 37 °C in PBS for 3 days, subsequently treated with 3-desoxy-collinoketone B (**8a**) and further incubation at 37 °C for another 3 days. 3-desoxy-collinoketone B (**8a**)-treated batch exhibited significantly reduced ThT-detected R3 aggregates level by 58.71% ($P < 0.0001$) compared to the untreated control batch for the identical total incubation duration (Fig**.** 7f). Additionally, 3-desoxy-collinoketone B (**8a**) demonstrated a dose-dependent inhibition of R3 aggregation and promoted the dissociation of pre-formed R3 aggregates (Supplementary Fig. 14).

To manifest whether the therapeutic effect on R3 could translate into cognitive improvement, we assessed the efficacy of 3-desoxy-collinoketone B (**8a**) on spatial working and hippocampal memory by performing a Y-maze test and novel object recognition (NOR) test utilizing an R3-infused mouse model with Alzheimer-like cognitive impairments. Considering that oligomeric forms are deemed more toxic and more closely linked to cognitive dysfunction than fibrillar forms[71], the preaggregation period was reduced from 3 days to 12 hours to produce oligomeric forms abundantly. R3 oligomers were preaggregated by incubating for 12 h, followed by treatment with 3-desoxy-collinoketone B (**8a**) and an additional 6 h incubation. The abundance of oligomeric forms in the samples was determined using a dot blot assay with a T22 (anti-tau oligomer) antibody. The sample co-incubated with 3-desoxy-collinoketone B (**8a**) for Y-maze test showed a 32.61% reduction in oligomer concentration compared to the untreated control sample (Fig. 7g). Importantly, the ThT assay, which detects β-sheet-rich fibrils, showed 83.75% ($P < 0.0001$) reduction of ThT fluorescence intensity in the 3-desoxy-collinoketone B (**8a**)-treated sample compared to the untreated R3 sample (Supplementary Fig. 15). These results imply that the reduced concentration of R3 oligomers is due to their dissociation into monomers and not their fibrillization, indicating that 3-desoxy-collinoketone B (**8a**) effectively dissociates R3 aggregates. In the case of sample for NOR test showed a 48.32% reduction in oligomer concentration and 22.06% reduction in β-sheet rich fibrils (Supplementary Fig. 15).

Based on these observations, 5 μL of each R3 incubated samples were injected into the intracerebroventricular (ICV) region of ICR mice (male, 7-week-old, n=9-10/group) for the Y-maze study and NOR study (Figs. 7h, 7i). In Y-maze test, the R3-infused group displayed a significant decrease in spontaneous alternation (alternation value: 49.92%) compared to the vehicle group (alternation value: 68.60%, $P = 0.0122$). In contrast, the 3-desoxy-collinoketone B (**8a**)-treated R3-infused group showed significant improvement in alternation levels (alternation value: 65.07%,

P = 0.0378), analogous to those of the vehicle group (Fig. 7h). Total arm entries were similar across all groups, indicating no differences in exploratory activity (Fig. 7h). Furthermore, in NOR study, the R3-infused group exhibited a significant reduction in both exploration time for novel object and the discrimination index value appear to -0.020. In contrast, the 3-desoxy-collinoketone B (**8a**)-treated R3-infused group showed a marked improvement, with prolonged exploration of the novel object and discrimination index of 0.058 (*P* = 0.0003), which was comparable to that of the vehicle-treated group (discrimination index 0.061, *P* = 0.0002) (Fig 7i). Collectively, these results indicate that 3-desoxy-collinoketone B (**8a**) exhibits both aggregation inhibition and disaggregation mechanisms that target key regions involved in PHF formation, suggesting its potential to alleviate cognitive deficits.

Comparison to Aβ and Tau dual modulator Necrostatin-1 (Nec-1)

We next evaluated the modulatory properties of 3-desoxy-collinoketone B (**8a**) on $A\beta_{42}$ and Tau comparison with the well-kwon dual modulator necrostatin-1 (Nec-1), which served as positive control.[72] [73] To assess and compare the aggregation inhibitory and aggregates dissociation efficacies of 3-desoxy collinoketone B (**8a**) with Nec-1, ThT assay were conducted under the previously described experimental conditions. Both Nec-1 and 3-desoxy-collinoketone B (**8a**) exhibited comparable inhibitory and dissociative effects on the $A\beta_{42}$. Notably, 3-desoxy -collinoketone B (**8a**) demonstrated superior inhibitory and dissociative activity against the R3 (Supplementary Fig. 16).

***In vitro and in vivo* ADME**

The plasma stability assay showed that 3-desoxy-collinoketone B (**8a**) remained stable for 2 h in both human and mouse plasma. In contrast, in the microsomal stability assay, it was unstable under metabolic conditions, with only 7.12% and 6.15% of the compound remaining after 30 min of incubation in human and mouse liver microsomes (0.5 mg/mL), respectively. In the Cytochrome P450(CYP) inhibition assay, the compound exhibited moderate inhibition of CYP2C19 and slight inhibition of CYP2D6 and CYP3A4 (Table. 1)

Following the intravenous (IV) administration of 3-desoxy -collinoketone B (**8a**) at 2 mg/kg, the compound was detected in brain tissue at 10.8 ± 3.6 ng/g and 8.9 ± 3.6 ng/g at 30 and 60 min, respectively. After oral (PO) administration at 30 mg/kg, 3-desoxy -collinoketone B (**8a**) was also detected in the brain tissue at 3.0 ± 3.2 ng/g 30 min and 3.4 ± 2.9 ng/g at 30 and 60 min,

respectively (Supplementary Fig 18). In plasma, 3-desoxy -collinoketone B (**8a**) concentrations in the IV group were 25.5 ± 9.9 ng/mL 5 min, 8.4 ± 1.3 ng/mL (30 min), 5.2 ± 2.8 ng/mL (60 min), and 4.1 ± 6.5 ng/mL (120 min). In the PO group, plasma concentrations were 19.0 ± 10.7 ng/mL (5 min), 1.5 ± 2.6 ng/mL (30 min), 0.8 ± 0.8 ng/mL (60 min), and 2.4 ± 2.5 ng/mL (120 min) (Supplementary Fig 18).

To conclude, the synthesis of 3-desoxy-collinoketone B (**8a**) was achieved via a stereoselective transannular [6+4] cycloaddition reaction as a key step. DFT calculations revealed that access to the collinoketone B framework with the (*R*)-configuration at C5 and C6=C7 *E*-configuration is not feasible via a thermal [6+4] cycloaddition reaction of the macrolactone precursor. AI-assisted binding pose modeling and molecular simulation revealed tighter binding of 3-desoxy-collinoketone B (**8a**) to Aβ and Tau aggregates compared to collinolactone (**1**), and further suggested that its binding perturbs key inter-fibrillar interactions, thereby promoting fibril destabilization. *In vitro* studies showed that 3-desoxy-collinoketone B (**8a**) reduces both Aβ and tau aggregations, while *in vivo* experiments demonstrated cognitive improvements in AD mouse models, underscoring the therapeutic relevance of the dual-function agent.

Notably, the improved lipophilicity of 3-desoxy-collinoketone B (**8a**) enabled the reduction of Aβ plaques in the cortex region, which is inaccessible by collinolactone (**1**).[23] The establishment of a scalable synthetic route to 3-desoxy-collinoketone B (**8a**) provides a critical foundation for the synthesis of the natural product, collinolactone (**1**), and also opens avenues for accessing its diverse derivatives. Furthermore, the convergent nature of our synthetic approach lends itself well to the generation of diverse structural analogs, enabling more in-depth structure-activity relationship (SAR) studies. Given the current limitations of monoclonal antibody therapies that target only Aβ, our findings provide a foundation for developing more accessible, cost-effective, and efficient treatments for AD.

The *in vivo* ADME results demonstrated that 3-desoxy-collinoketone B (**8a**) was detectable in brain tissue following both IV and PO administration, indicating that the compound is capable of penetrating the BBB. However, the relatively low plasma concentrations observed in both dosing routes limited systemic exposure. Consistent with this observation, the *in vitro* microsomal stability assay revealed low metabolic stability in both human and mouse liver microsomes, indicating that 3-desoxy-collinoketone B (**8a**) undergoes rapid metabolic clearance. These finding collectively suggest that structural optimization of 3-desoxy-collinoketone B (**8a**) is required to enhance its metabolic stability and systemic bioavailability while maintaining brain permeability.

Methods

Peptide Preparations

Synthesis of $A\beta_{42}$

Synthesized $A\beta_{42}$ acquired by Fmoc solid phase peptide synthesis (Fmoc-SPPS) and purification as previously reported.

Labeling Flamma 552 to $A\beta_{42}$

After synthesizing $A\beta_{42}$, 2.2 mmol of Flamma 552 carboxylic acid, 2.2 mmol of DIC, and 1.0 M of Oxyma were added to the $A\beta_{42}$ and reacted for 48 h at RT.

Labeling FITC to $A\beta_{42}$

After synthesizing $A\beta_{42}$, 0.05 mmol of FITC and 0.3 mmol of DIEA were added to the $A\beta_{42}$, and reacted for 6 h at RT.

Synthesis of Tau R3

Synthesized tau (306-336) R3, Ac-VQIVYKPVDLSKVTSKCGSLGNIHHKPGGGQ-NH_2 was acquired in-house by Fmoc-SPPS. For C-terminal amidation, 5 eq. of Fmoc-Rink amide-linker, 5 eq. of DIC, and 5 eq. of Oxyma were dissolved in DMF and added to DMF swelled Polystyrene AM NH_2 resin. After 2 h of the activation on a shaker, amino acids were sequentially coupled by the automated peptide synthesizer (Liberty Blue, CEM, USA). For amino acid coupling reagents, 1.0 M Oxyma and 1.0 M DIC were used. N-terminal Fmoc protecting groups were removed by 20% piperidine (1:4, piperidine/DMF, v/v) in between every coupling step. Lastly, N-terminal acetylation was conducted by adding mixture of 40 eq. of acetic anhydride and 4 eq. of DIEA dissolved in an appropriate amount of DMF. This reaction was performed for 3 h on a shaker. After synthesis, the final peptides were cleaved from the resin by 92.5% TFA (92.5:2.5:2.5:2.5, TFA/TIS/deionized water/DODT, v/v/v/v) for 4 h on a shaker. TFA was removed via a rotary evaporator, and the peptides were isolated and obtained through cold ether precipitation by centrifugation (3000 rpm, 15 min, twice).

Peptide Analysis and Purification

To analyze and purify synthesized peptides, reverse-phase high-performance liquid chromatography (RP-HPLC) (1220; Agilent) and electrospray ionization mass spectroscopy (ESI-MS) (6120; Agilent) were carried out using binary gradients of solvent A (0.1% TFA in deionized

water) and B (0.09% TFA in ACN). Kinetex 5 µm C18 150 × 4.6 mm column and Phenomenex jupiter 10 µm C18 250 × 21.2 mm column were used for the analysis and purification, respectively. UV detection was conducted at 230 nm.

Thioflavin T (ThT) Assay

$A\beta_{42}$ Inhibition and Disaggregation

ThT fluorescence was used to assess the inhibitory/dissociative effects of 3-desoxy-collinoketone B against $A\beta_{42}$ aggregation/aggregates. In house synthesis $A\beta_{42}$ was dissolved in DMSO (4 mM, 100% DMSO) and diluted to 100-fold in deionized water to make 40 µM $A\beta_{42}$ stocks (1% DMSO). 3-desoxy-collinoketone B (**8a**) was dissolved in DMSO (10 mM, 100% DMSO) and diluted with deionized water to make 1 mM (20% DMSO). To assess the ability of 3-desoxy-collinoketone B (**8a**) to inhibit Aβ aggregation, 20 µM of $A\beta_{42}$ were incubated with 500 µM of 3-desoxy-collinoketone B (**8a**) for a day at 37 °C, at final DMSO concentration of 10.5% DMSO in deionized water. For $A\beta_{42}$ fibril dissociation assay, 40 µM $A\beta_{42}$ stocks (1% DMSO) was incubated for a day at 37 °C to obtain pre-aggregated $A\beta_{42}$ fibrils. 500 µM of 3-desoxy-collinoketone B (**8a**) was treated to pre-aggregated $A\beta_{42}$ fibrils and incubated for additional one day at 37 °C.

Tau K18 Inhibition and Disaggregation

ThT fluorescence was used to assess the inhibitory/dissociative effects of 3-desoxy-collinoketone B against Tau K18 aggregation/aggregates. Tau K18 was dissolved in PBS (1 mg/mL) and 3-desoxy-collinoketone B (**8a**) was dissolved in DMSO (10 mM, 100% DMSO). To induce aggregation of tau, 2 mg/mL of heparin and 10 mM of DTT were added to the tau protein at final concentration of 0.1 mg/mL and 100 µM each. To assess the ability of 3-desoxy-collinoketone B to inhibit Tau K18 aggregation, 35 µM of Tau K18 was incubated with 1000 µM of 3-desoxy-collinoketone B (**8a**) for 3 days at 37 °C, at final DMSO concentration of 10% DMSO in PBS. For Tau K18 aggregates dissociation assay, Tau K18 was incubated for 3 days at 37 °C to obtain pre-aggregated Tau K18. 1000 µM of 3-desoxy-collinoketone B (**8a**) was treated to pre-aggregated Tau K18 and incubated for additional 3 days at 37 °C.

Tau Repeat domain 3 (R3) Inhibition and Disaggregation

ThT fluorescence was used to assess the inhibitory/dissociative effects of 3-desoxy-collinoketone B against Tau repeat domain 3 (R3) aggregation/aggregates. R3 was dissolved in PBS (70 µM) and 3-desoxy-collinoketone B (**8a**) was dissolved in DMSO (10 mM, 100% DMSO). To assess the ability of 3-desoxy-collinoketone B (**8a**) to inhibit R3 aggregation, 35 µM of R3 was incubated

with 1000 μM of 3-desoxy-collinoketone B (**8a**) for 3 days at 37 °C, at final DMSO concentration of 10% DMSO in PBS. For R3 aggregates dissociation assay, R3 was incubated for 3 days at 37 °C to obtain pre-aggregated R3. 1000 μM of 3-desoxy-collinoketone B (**8a**) was treated to pre-aggregated R3 and incubated for additional 3 days at 37 °C.

After the incubations, 25 μL of each sample was loaded into half-area 96-well black plate (3694, Corning Inc., USA) in triplicate, and 75 μL of ThT solution (5 μM in 50 mM glycin buffer, pH 8.5) was added to each well. The fluorescence intensity of β-sheet bound ThT was measured at 450 nm (excitation) and 485 nm (emission) using a microplate reader (Infinite M200 Pro, TECAN, USA).

Amyloid Aggregate Assay (A3)

$A\beta_{42}$ oligomers dissociation activity

$A\beta_{42}$ containing a cysteine residue at the C-terminal was synthesized by the automated microwave peptide synthesizer (Liberty Blue, CEM) as previously reported methods. The synthesized peptide was dissolved in DMSO and then diluted with binding buffer (0.1 M sodium phosphate, 0.15 M sodium chloride, 10 mM EDTA, pH 7.2) to prepare 50 μg/mL peptide solution. 100 μL volume of peptide solution was dispensed into each well of the maleimide-activated microplate and shaken for 2 h at RT to immobilized for fabricating an amyloid aggregate assay (A3). For sealing the unreacted maleimide groups, 200 μL of cysteine solution (10 μg/mL in binding buffer) was added and incubated for an hour at RT with shaking. Thereafter, 10 μM flamma552-labeled $A\beta_{42}$ was prepared by dilution with deionized water (10% DMSO) and incubated for 8 h at 37 °C. The fluorescence intensity was measured at 555/580 nm (excitation/emission) to establish the fluorescence baseline for every well. 3-desoxy-collinoketone B (500 μM in binding buffer) was dispensed into the well and incubated for a day at RT with shaking. After incubation, the fluorescence intensity was assessed again at 555/580 (excitation/emission), and the difference between the baseline and remeasured fluorescence intensity was utilized to calculate the alteration in the fluorescence intensity by 3-desoxy-collinoketone B (**8a**) treatment. Between each step, the plate was washed 3 times with 200 μL of washing buffer (0.1 M sodium phosphate, 0.15 M sodium chloride, and 0.05% Tween-20, pH 7.2).

Mapping Amyloid Plate (MAP)

To elucidate the targeting region in $A\beta_{42}$ of 3-desoxy -collinoketone B (**8a**), plate wells with immobilized $A\beta_{42}$ or each $A\beta_{42}$ hexamer were treated with 100 μL of peptide solutions containing

FITC-labeled $A\beta_{42}$ (10 μM, 5% DMSO in wash buffer) either alone or in combination with 500 μM 3-desoxy -collinoketone B (8a). Plates were incubated at 37 °C for 1 day, followed by 5 washes with 200 μL of wash buffer. Each well received 100 μL of binding buffer, and fluorescence intensities of control and 3-desoxy -collinoketone B (8a)-treated wells were measured with excitation at 495 nm and emission at 525 nm.

Blood Brain Barrier (BBB) Permeability Test

Parallel artificial membrane permeability assay studies were performed using PAMPA-BBB kit (BioAssay Systems, PMBBB-096) according to the manufacturer's instructions. 3-desoxy-collinoketone B (**8a**) and control (high permeability control, promazine hydrochloride; low permeability control, diclofenac) stock solutions were prepared in DMSO, which were then diluted with PBS (pH 7.4) to a final concentration of 500 μM. The polyvinylidene difluoride (PVDF) membranes on each donor plate well were coated by adding 5 μL of the BBB lipid solution. Then, 200 μL of 3-desoxy-collinoketone B (**8a**) and controls were added to each well of the donor plate (n = 2, all the samples were duplicated) and each well of the acceptor plate was filled with 300 μL of PBS. The donor plate was placed on the acceptor plate to form a sandwich, and separate tubes were prepared for equilibrium standards. The sandwich plate and equilibrium standards were incubated at RT for 18 h without stirring. 100 μL of equilibrium standard, acceptor, and donor solutions were transferred to UV plates and the absorbance spectrums of the solutions were measured from 200 nm to 500 nm in 10 nm intervals using a plate reader (SpectraMax M2e). Effective permeability (P_e) for samples was calculated using the data analysis equation specified in the manufacturer's instruction of BioAssay Systems.

Animal Preparation

5XFAD mice (strain name: B6SJL-Tg(APPSwFILon,PSEN*M146L*L286V)6799Vas/-Mmjax) expressing the Swedish (K670N/M671L), Florida (I716V), and London (V717I) mutation in APP and the M146L and L286V mutation in PSEN1), and wild-type mice (C57BL/6 x SJL) were originally obtained from the Jackson Laboratory (Bar Harbor, Maine, USA). PS19 mice (strain name: B6;C3-Tg(Prnp-MAPT*P301S)PS19Vle/J expressing the MAPT P301S, and wild-type mice (C57BL/6 x C3H) were originally obtained from the Jackson Laboratory (Bar Harbor, Maine, USA). Heterozygous transgenic mice were maintained through cross-breeding with the wild-type mice, and the genotype of all mice were confirmed via PCR analysis of tail DNA following the standard PCR condition from the Jackson Laboratory. 7-week-old male ICR mice were acquired from Orient Bio Inc. (Republic of Korea).

All mice were housed in a laboratory animal room and were maintained under controlled temperature (18 to 23 °C), humidity (40% to 60%), and an alternating 12-hour light-dark cycle. Access to food and water were available ad libitum. All animal experiments were carried out in accordance with the National Institutes of Health guide for the care and use of laboratory animals. Protocols were approved by Institutional Animal Care and Use Committee (IACUC) of the Yonsei Laboratory Animal Research Center. (Republic of Korea, IACUC-A-202404-1837-01)

Drug Administration

5XFAD Mouse Model (Short-term dosing)

6.4-month-old female 5XFAD mice and littermate wildtype were utilized to test in vivo efficacy. 3-desoxy-collinoketone B (30 mg/kg/day) and vehicle (10% DMSO, 10% Tween80 in PBS) were daily administered according to their body weight via oral gavage (PO) for 5 days. After a day on completion of drug administration, all mice were anesthetized and sacrificed at the age of about 6.5 months.

5XFAD Mouse Model (Long-term dosing)

8.0-month-old male 5XFAD mice (n = 4/group) and littermate wildtype were utilized to test in vivo efficacy. 3-desoxy-collinoketone B (**8a**) (30 mg/kg/day) and vehicle (10% DMSO, 10% Tween80 in PBS) were administered three times per week according to their body weight via oral gavage (PO) for one month. After a day on completion of drug administration, all mice were anesthetized and sacrificed at the age of about 9.0 months.

PS19 Mouse Model

7.5-month-old female PS19 mice and littermate wildtype were utilized to test in vivo efficacy. 3-desoxy-collinoketone B (**8a**) (30 mg/kg/day) and vehicle (10% DMSO, 10% Tween80 in PBS) were administered twice a week according to their body weight via oral gavage (PO) for 3 weeks. After a day on completion of drug administration, all mice were anesthetized and sacrificed at the age of about 8.5 months.

Thioflavin S (ThS) Staining

Mice brains were recovered after perfusion with 0.9% saline, and each hemisphere was fixed with 4% paraformaldehyde for 24 h. Fixed brains were immersed in 30% sucrose for two days, and brain tissues were sectioned with 25-μm thickness using cryostat (CM1860, Leica, Germany). Brain tissues were mounted onto glass slides and antigen retrieval was performed by submerging

slides in 1% SDS and unspecific binding was blocked through incubation in 5% horse serum in PBS-T for one hours at RT. To detect Aβ plaques, brain slides were stained with 1.5 mM ThS in 50% ethanol for 7 minutes in duplicate and de-stained with 80% ethanol, and PBS, for one minute each. All images were taken using a fluorescence microscope (DM-2500, Leica) and the Aβ plaques counts in the hippocampus were analyzed by Image J software (NIH).

Preparation of Tau repeat domain 3 (R3)-infused Acute AD Mouse Model

Prior to the behavior study, purified R3 was dissolved in 1,1,1,3,3,3-hexafluoro-2-propanol (HFIP) and sonicated for 15 min, and then removed the HFIP completely via evaporation with nitrogen to dissolve any aggregates and make the peptides homogeneous. To prepare pre-aggregated oligomer abundant R3 aggregates, HFIP-treated R3 were incubated for 12 h at 37 °C, after that with/without 3-desoxy-collinoketone B (**8a**) treated samples were additionally incubated for 6 h at 37 °C. The three samples were prepared as follows: vehicle (10% DMSO in PBS), R3 aggregates without 3-desoxy-collinoketone B treatment (10% DMSO in PBS), and R3 aggregates with 3-desoxy-collinoketone B treatment (10% DMSO in PBS).

Immunoblotting

Brain Lysis

The cortical and hippocampal regions were collected from the brains of the experimented wild-type, 5XFAD, and PS19 mice. Frozen brain tissues were homogenized in RIPA buffer containing protease and phosphatase inhibitor cocktails, then incubated on ice for 30 minutes. Lysates were centrifuged at 18,500 x g, at 4 °C for 30 minutes. Supernatants were collected and concentrations of lysates were quantified by the BCA assay kit.

Dot Blot Analysis

5 µg of brain lysates were spotted onto a nitrocellulose (NC) membrane in duplicate and completely dried. Membrane was blocked with 5% skim milk in tris-buffered saline with 0.1% Tween-20 detergent (TBS-T) and treated with primary antibodies overnight at 4 °C. Primary anti-Aβ 6E10 antibody (1:1000, BioLegend, USA, catalog# SIG-39320) and anti-oligomer A11 antibody (1:1000, Invitrogen, USA, catalog# AHB0052) were used to visualize total Aβ and oligomeric Aβ. Primary anti-tau oligomer T22 antibody (1:1000, Millipore Corporation, USA, catalog# ABN454) were used to visualize oligomeric Tau. Following the overnight incubation, the membranes were incubated with HRP-conjugated IgG antibodies for 1 h and developed utilizing

ECL solutions (Thermo Fisher Scientific). All washing steps were performed three times using TBS-T for 5 minutes each.

Western Blot Analysis

20 µg of brain lysates were loaded to SDS-PAGE gel and transferred to a NC membrane. Membrane was blocked with 5% skim milk in TBS-T and treated with primary antibodies overnight at 4 °C. Then, detected by HRP-conjugated secondary antibodies and developed with the ECL solution. The protein levels for each mice group were quantified using Image J and were organized into graphical data with Prism 10.0 by normalization to β-actin.

Behavior Tests

Y-maze

Y-maze tests were performed to assess cognitive alteration of short-term spatial working memory (by spontaneous alternation) and exploratory activity (by number of total arm entries). Y-maze is a Y-shaped maze (40 cm long, 10 cm wide, 12 cm high) with three symmetrical arms at a 120° angle from each other. Each mouse was placed at one arm to freely move through the maze during a 5-minute session. The number of arm entries and triads were recorded to calculate the alternation percentage. An entry of a mouse was considered when all four limbs were withing the arm, passing the middle circle region.

Novel Object Recognition (NOR)

NOR was conducted for three days consisting of habituation, training, and testing. Mice behavior was assessed in an open-field arena (40 x 40 x 40 cm, matte acrylic) and cleaned with 70% ethanol followed by deionized water (DW) after every trial. For the first day, each mouse was placed in the middle of the arena and allowed to freely explore the empty arena for five minutes. For the second day, two identical objects were placed 10 cm from the wall in opposite quadrants. Mice were allowed to explore for 10 minutes. Exploration was defined as active investigation with nose oriented toward the object at 2 cm (sniffing, touching, climbing, or grooming near the object was not considered exploration). After a 24-h interval, one familiar object was replaced with a novel object. Orientation of the objects were counterbalanced withing each group to control for side and object biases. Mice were examined for 10 minutes for the last time. Exploration time for each object was recorded until it met the minimum time needed (20 s). Discrimination index was calculated by subtracting familiar object exploration (s) from novel object exploration (s) and diving it by total exploration during testing (s).

In Vivo Toxicity Test

B6SJL Mouse Model (Long-term dosing)

8.0-month-old male wildtype mice (n=8) were utilized to test in vivo toxicity. 3-desoxy-collinoketone B (**8a**) (30 mg/kg/day) was administered three times per week according to their body weight via oral gavage (PO) for one month. Body weight and food intake were recorded prior to and weekly during the administration period. After a day on completion of drug administration, all mice were anesthetized and sacrificed at the age of about 9.0 months.

In Vitro ADME

Microsomal Stability Assay

Test compound was added to be 1 μM in 0.5 mg/mL liver microsomes specific for human and mouse (Corning, AZ, USA) in 0.1 M phosphate buffer (pH 7.4) and pre-incubated for 5 minutes at 37 °C. Reaction was initiated by addition of NADPH and incubated for 30 minutes at 37 °C. Then, acetonitrile (Sigma-Aldrich, MO, USA) containing 1 μM chloropropamide (TRC, Toronto, Canada) was added to terminate reaction and supernatant after centrifugation at 21,200 x g for 5 minutes at 4 °C was loaded onto LC-MS/MS system (TSQ Vantage, Thermo Fisher Scientific, MA, USA). Only pre-incubated sample for 5 minutes without NADPH was used as control, which defined as 100% activity, and then, microsomal stability of test compound was calculated as percent remaining compared to control.

CYP (Cytochrome P450) inhibition Assay

CYP inhibition was assessed by measuring metabolites of CYP450 isoform specific substrates and all chemicals were purchased from Sigma-Aldrich. 10 μM of test compound was pre-incubated for 5 minutes in 0.25 mg/ml human liver microsomes and the mixture of CYP specific probes, which consisted of 20 μM penacetin, 3.5 μM bupropion, 1 μM amodiaquine, 1 μM diclofenac, 40 μM S-mephenytoin, 2 μM dextromethorphan, 0.1 μM midazolam and 2 μM testosterone in 0.1 M phosphate buffer (pH 7.4). Reaction was initiated by addition of NADPH (Promega, WI, USA) and incubated for 10 minutes at 37 °C. Then, reaction was terminated by addition of acetonitrile containing 1 μM chloropropamide (TRC, Toronto, Canada) as internal standard for LC-MS/MS analysis. After centrifugation of reaction mixture at 21,200 x g for 5 minutes at 4 °C, supernatant was injected into an LC-MS/MS system. Reaction sample without test compound was presented as control and its activity was defined as 100%. Then, CYP enzyme activity was calculated as percent of control activity. All experiments were performed in duplicates.

Plasma stability assay

Test compound was spiked into human or mouse plasma (Biochemed, VA, USA) to be 10 μM, and incubated at 37 °C with shaking for 0, 30, or 120 minutes. After incubation, 100 μL of each sample was transferred into a new 1.5 mL tube containing 200 μL of acetonitrile with 1 μM chloropropamide as internal standard. In order to remove proteins and debris, vortexing and centrifugation at 21,200 x g for 10 minutes at 4 °C were conducted subsquently. Then, the amount of test compound in sample was determined as area ratio (area of analyte / area of internal standard) measured using LC-MS/MS system. And, stability data was presented as % remaining compared to control (zero minute).

***In Vivo* ADME**

7.0-week-old male ICR mice (n = 3 per time point) were utilized for *in vivo* bioanalysis studies. 3-desoxy-collinoketone B (**8a**) was administered either orally (30 mg/kg; 10% DMSO, 10% Tween80 in PBS) or intravenously (2 mg/kg; 10% DMSO, 5% Tween 80 in PBS), with each administration route performed in separate groups. Blood samples were collected at 5, 30, 60, and 120 min after dosing and brain samples were obtained at 30 and 60 min.

For quantitative analysis in plasma, 20 μL plasma was transferred into an e-tube and 100 μL acetonitrile containing 2.5 nM terfenadine as an internal standard was added. After vortexing, sample was centrifuged at 15,000 rpm for 10 minutes at 4 ℃ and supernatant was loaded onto LC-MS/MS system (Triple Quad 6500 plus system, AB Sciex, USA). Calibration range of the analyte in plasma was between 1 ng/mL and 200 ng/mL. Brain tissue was homogenized after addition of 5 volumes (mL) PBS (pH 7.4) of tissue weight (g) and homogenate was used for quantitative analysis. After vortexing samples, 100 μL brain homogenate was aliquoted into a new e-tube and mixed with 200 μL acetonitrile containing 2.5 nM terfenadine. Then, the sample was centrifuged at 21,200 x g for 10 minutes at 4 °C and supernatant was loaded onto LC-MS/MS system for analysis. Calibration range of the analyte in brain homogenates was between 0.5 ng/mL and 50 ng/mL, and the amount was calculated by multiplication of dilution factor for homogenization (X5).

Statistical Analyses

All data were presented graphically with GraphPad Prism 10.0 or Seaborn (v0.13.2). Statistical analyses were conducted using a two- or one-tailed unpaired *t*-tests or one-way ANOVA followed

by Bonferroni's post-hoc comparisons (*P < 0.05, **P < 0.01, ***P < 0.001, ****P < 0.0001, and other comparisons not significant). Error bars denote either the standard error of the mean (±SEM) or the 95% confidence interval, as specified for each experiment.

Data Availability

The data that support the findings of this study are available within the paper and its supplementary information files. Source data underlying the figures are provided with this paper. CCDC 2391862 contains the supplementary crystallographic data for compound **8a**. These data can be obtained free of charge from The Cambridge Crystallographic Data Centre via [www.ccdc.cam.ac.uk/structures].

Code Availability

The source codes for the models used in this study are publicly available at the following repositories: DiffDock-L [https://github.com/gcorso/DiffDock], NeuralPLexer2 [https://github.com/zrqiao/NeuralPLexer], and PIGNet2 [https://github.com/mseok/PIGNet2].

References

1. Yu, P., Patel, A. & Houk, K. N. Transannular [6 + 4] and ambimodal cycloaddition in the biosynthesis of heronamide A. *J. Am. Chem. Soc.* **137**, 13518–13523 (2015).
2. Chen, N., Zhang, F., Wu, R. & Hess, B. A., Jr. Biosynthesis of spinosyn A: A [4 + 2] or [6 + 4] cycloaddition? *ACS Catal.* **8**, 2353–2358 (2018).
3. Kanoh, N. et al. Asymmetric total synthesis of heronamides A-C: Stereochemical confirmation and impact of long-range stereochemical communication on the biological activity. *Chem. Eur. J.* **22**, 8586–8595 (2016).
4. Zhang, B. *et al.* Enzyme-catalysed [6+4] cycloadditions in the biosynthesis of natural products. *Nature* **568**, 122–126 (2019).
5. Wang, K. B. *et al.* A [6+4]-cycloaddition adduct is the biosynthetic intermediate in streptoseomycin biosynthesis. *Nat. Commun.* **12**, 2092 (2021).
6. Schiewe, H. J. & Zeeck, A. Cineromycins, gamma-butyrolactones and ansamycins by analysis of the secondary metabolite pattern created by a single strain of Streptomyces. *J. Antibiot. (Tokyo)* **52**, 635–642 (1999).
7. Bode, H. B., Bethe, B., Höfs, R. & Zeeck, A. Big effects from small changes: possible ways to explore nature's chemical diversity. *Chembiochem* **3**, 619–627 (2002).
8. Schmid, J. C. *et al.* The Structure of Cyclodecatriene Collinolactone, its Biosynthesis, and Semisynthetic Analogues: Effects of Monoastral Phenotype and Protection from Intracellular Oxidative Stress. *Angew. Chem. Int. Ed.* **60**, 23212–23216 (2021).
9. Decker, R. L., Schray, D., Pfeffer, H. I., Grond, S. & Wagner, J. P. Conformations and rearrangements of collinolactone - experiments and theory on a dynamic cyclodecatriene. *Chem. Eur. J.* **30**, e202303435 (2024).
10. Heo, S. *et al.* Synthesis of 3-dehydroxy-5-*epi*-collinoketone and its cognitive benefits by reducing aggregates of amyloid-β and tau preprint at Chemrxiv https://chemrxiv.org/doi/full/10.26434/chemrxiv-2025-cqswq (2025)
11. Reiter, H. *et al.* Synthesis of Collinoketones via Biomimetic [6 + 4] Cycloaddition *J. Am. Chem. Soc*. **147**, 43205–43212 (2025)
12. Hardy, J. Alzheimer's disease: the amyloid cascade hypothesis: an update and reappraisal. *J. Alzheimers. Dis.* **9**, 151–153 (2006).
13. Yao, W., Yang, H. & Yang, J. Small-molecule drugs development for Alzheimer's disease. *Front. Aging Neurosci.* **14**, 1019412 (2022).
14. Cummings, J. Zhou, Y., Lee, G., Zhong, K., Froseca, J., & Cheng, F. Alzheimer's disease

drug development pipeline: 2024. *Alzheimers. Dement.* **10**, e12465 (2024).

15. Singh, B., Day, C. M., Abdella, S. & Garg, S. Alzheimer's disease current therapies, novel drug delivery systems and future directions for better disease management. *J. Control. Release* **367**, 402–424 (2024).
16. Rashad, A. *et al.* Donanemab for Alzheimer's disease: A systematic review of clinical trials. *Healthcare (Basel)* **11**, 32 (2022).
17. Wojtunik-Kulesza, K., Rudkowska, M. & Orzeł-Sajdłowska, A. Aducanumab—Hope or Disappointment for Alzheimer's Disease. *Int. J. Mol. Sci.* **24**, 4367 (2023).
18. Cummings, J. L. *et al.* The therapeutic landscape of tauopathies: challenges and prospects. *Alzheimers. Res. Ther.* **15**, 168 (2023).
19. Busche, M. A. & Hyman, B. T. Synergy between amyloid-β and tau in Alzheimer's disease. *Nat. Neurosci.* **23**, 1183–1193 (2020).
20. Pickett, E. K. *et al.* Amyloid Beta and Tau Cooperate to Cause Reversible Behavioral and Transcriptional Deficits in a Model of Alzheimer's Disease. *Cell Rep.* **29**, 3592–3604.e5 (2019).
21. Pasieka, A. *et al.* Dual Inhibitors of Amyloid-β and Tau Aggregation with Amyloid-β Disaggregating Properties: Extended In Cellulo, In Silico, and Kinetic Studies of Multifunctional Anti-Alzheimer's Agents. *ACS Chem. Neurosci.* **12**, 2057–2068 (2021).
22. Malafaia, D., Albuquerque, H. M. T. & Silva, A. M. S. Amyloid-β and tau aggregation dual-inhibitors: A synthetic and structure-activity relationship focused review. *Eur. J. Med. Chem.* **214**, 113209 (2021).
23. Gandini, A. *et al.* Discovery of Dual Aβ/Tau Inhibitors and Evaluation of Their Therapeutic Effect on a Drosophila Model of Alzheimer's Disease. *ACS Chem. Neurosci.* **13**, 3314–3329 (2022).
24. Kwon, Y. *et al.* Rhizolutin, a Novel 7/10/6-Tricyclic Dilactone, Dissociates Misfolded Protein Aggregates and Reduces Apoptosis/Inflammation Associated with Alzheimer's Disease. *Angew. Chem. Int. Ed.* **59**, 22994–22998 (2020).
25. Kim, T., Lee, S. I., Kim, S., Shim, S. Y. & Ryu, D. H. Total synthesis of PGF2α and 6,15-diketo-PGF1α and formal synthesis of 6-keto-PGF1α via three-component coupling. *Tetrahedron* **75**, 130593 (2019).
26. Roethle, P. A., Chen, I. T. & Trauner, D. Total synthesis of (-)-archazolid B. *J. Am. Chem. Soc.* **129**, 8960–8961 (2007).
27. Roulland, E. & Ermolenko, M. S. Synthesis of the C12-C19 fragment of (+)-peloruside A through a diastereomer-discriminating RCM reaction. *Org. Lett.* **7**, 2225–2228 (2005).

28. Surendra, K., Rajendar, G. & Corey, E. J. Useful catalytic enantioselective cationic double annulation reactions initiated at an internal π-bond: method and applications. *J. Am. Chem. Soc.* **136**, 642–645 (2014).
29. Ding, X.-B., Furkert, D. P. & Brimble, M. A. 2-Nitropyrrole cross-coupling enables a second generation synthesis of the heronapyrrole antibiotic natural product family. *Chem. Commun.* **52**, 12638–12641 (2016).
30. Schomaker, J. M.; Pulgam, V. R.; Borhan, B. Synthesis of Diastereomerically and Enantiomerically Pure 2,3-Disubstituted Tetrahydrofurans Using a Sulfoxonium Ylide. *J. Am. Chem. Soc.* **2004**, *126*, 42, 13600–13601.
31. Tseng, N.-W. & Lautens, M. Rhodium-catalyzed vinylcyclopropanation/cyclopentenation of strained alkenes via a sequential carborhodation process. *J. Org. Chem.* **74**, 2521–2526 (2009).
32. Paterson, I., Yeung, K.-S. & Smaill, J. -B. The Horner-Wadsworth-Emmons reaction in natural products synthesis: Expedient construction of complex (E)-enones using barium hydroxide. *Synlett* **10**, 774–776 (1993).
33. Symkenberg, G. & Kalesse, M. Structure elucidation and total synthesis of kulkenon. *Angew. Chem. Int. Ed.* **53**, 1795–1798 (2014).
34. Balas, L. *et al.* Linotrins: Omega-3 oxylipins featuring an E,Z,E conjugated triene motif are present in the plant kingdom and alleviate inflammation in LPS-challenged microglial cells. *Eur. J. Med. Chem.* **231**, 114157 (2022).
35. Oka, N., Yamada, T., Sajiki, H., Akai, S. & Ikawa, T. Aryl boronic esters are stable on silica gel and reactive under Suzuki-Miyaura coupling conditions. *Org. Lett.* **24**, 3510–3514 (2022).
36. Gade, N. R. & Iqbal, J. Stereoselective formal synthesis of macrolidecore of migrastatin using late stage C–H oxidation. *Tetrahedron Lett.* **54**, 4225–4227 (2013).
37. Kim, H. J. *et al.* Chemoenzymatic synthesis of spinosyn A. *Angew. Chem. Int. Ed.* **53**, 13553–13557 (2014).
38. Pracht, P.; Bohle, F.; Grimme, S.; Automated exploration of the low-energy chemical space with fast quantum chemical methods, Phys. Chem. Chem. Phys., **22**, 7169-7192 (2020).
39. K. Lee, J. Lee, S. Park & W. Y. Kim. J. Chem. Theory Comput. **21**, 2487–2500 (2025).
40. Sperling, R. A. *et al.* Toward defining the preclinical stages of Alzheimer's disease: recommendations from the National Institute on Aging-Alzheimer's Association workgroups on diagnostic guidelines for Alzheimer's disease. *Alzheimers. Dement.* **7**, 280–292 (2011).
41. Burley, S. K. *et al.* Updated resources for exploring experimentally-determined PDB structures and Computed Structure Models at the RCSB Protein Data Bank. *Nucleic Acids Res.* **53**,

D564–D574 (2025).

42. Lührs, T. *et al.* 3D structure of Alzheimer's amyloid-beta(1-42) fibrils. *Proc. Natl. Acad. Sci. U. S. A.* **102**, 17342–17347 (2005).
43. Fitzpatrick, A. W. P. *et al.* Cryo-EM structures of tau filaments from Alzheimer's disease. *Nature* **547**, 185–190 (2017).
44. Corso, G., Stärk, H., Jing, B., Barzilay, R. & Jaakkola, T. DiffDock: Diffusion steps, twists, and turns for molecular docking. *arXiv [q-bio.BM]* (2022).
45. Corso, G. *et al.* Deep confident steps to new pockets: Strategies for docking generalization. *arXiv [q-bio.BM]* (2024).
46. Chen, S., Zheng, J. & Li, J. The impact of sample size after sampling on the accuracy of machine learning models. in *2024 International Conference on Computers, Information Processing and Advanced Education (CIPAE)* 61–66 (IEEE, 2024).
47. Koes, D. R., Baumgartner, M. P. & Camacho, C. J. Lessons learned in empirical scoring with smina from the CSAR 2011 benchmarking exercise. *J. Chem. Inf. Model.* **53**, 1893–1904 (2013).
48. Trott, O. & Olson, A. J. AutoDock Vina: improving the speed and accuracy of docking with a new scoring function, efficient optimization, and multithreading. *J. Comput. Chem.* **31**, 455–461 (2010).
49. Salentin, S., Schreiber, S., Haupt, V. J., Adasme, M. F. & Schroeder, M. PLIP: fully automated protein-ligand interaction profiler. *Nucleic Acids Res.* **43**, W443–7 (2015).
50. Schake, P., Bolz, S. N., Linnemann, K. & Schroeder, M. PLIP 2025: introducing protein-protein interactions to the protein-ligand interaction profiler. *Nucleic Acids Res.* **53**, W463–W465 (2025).
51. Qiao, Z., Nie, W., Vahdat, A., Miller, T. F., III & Anandkumar, A. State-specific protein–ligand complex structure prediction with a multiscale deep generative model. *Nat. Mach. Intell.* **6**, 195–208 (2024).
52. Bouysset, C. & Fiorucci, S. ProLIF: a library to encode molecular interactions as fingerprints. *J. Cheminform.* **13**, 72 (2021).
53. Gremer, L. *et al.* Fibril structure of amyloid-β(1-42) by cryo-electron microscopy. *Science* **358**, 116–119 (2017).
54. Im, D. *et al.* Decoding the roles of amyloid-β (1-42)'s key oligomerization domains toward designing tope-specific aggregation inhibitors. *JACS Au* **3**, 1065–1075 (2023).
55. Kunach, P. *et al.* Cryo-EM structure of Alzheimer's disease tau filaments with PET ligand MK-6240. *Nat. Commun.* **15**, 8497 (2024).

56. LeVine, H., 3rd. Quantification of beta-sheet amyloid fibril structures with thioflavin T. *Methods Enzymol.* **309**, 274–284 (1999).
57. Ferreira, S. T. & Klein, W. L. The Aβ oligomer hypothesis for synapse failure and memory loss in Alzheimer's disease. *Neurobiol. Learn. Mem.* **96**, 529–543 (2011).
58. Cho, I. *et al.* Immobilized amyloid hexamer fragments to map active sites of amyloid-targeting chemicals. *ACS Chem. Neurosci.* **14**, 9–18 (2023).
59. von Bergen, M., Barghorn, S., Biernat, J., Mandelkow, E.-M. & Mandelkow, E. Tau aggregation is driven by a transition from random coil to beta sheet structure. *Biochim. Biophys. Acta* **1739**, 158–166 (2005).
60. Jakes, R., Novak, M., Davison, M. & Wischik, C. M. Identification of 3- and 4-repeat tau isoforms within the PHF in Alzheimer's disease. *EMBO J.* **10**, 2725–2729 (1991).
61. Ambadipudi, S., Biernat, J., Riedel, D., Mandelkow, E. & Zweckstetter, M. Liquid-liquid phase separation of the microtubule-binding repeats of the Alzheimer-related protein Tau. *Nat. Commun.* **8**, 275 (2017).
62. Vergara, C. *et al.* Amyloid-β pathology enhances pathological fibrillary tau seeding induced by Alzheimer PHF in vivo. *Acta Neuropathol.* **137**, 397–412 (2019).
63. He, Z. *et al.* Amyloid-β plaques enhance Alzheimer's brain tau-seeded pathologies by facilitating neuritic plaque tau aggregation. *Nat. Med.* **24**, 29–38 (2018).
64. Nelson, P. T., Braak, H. & Markesbery, W. R. Neuropathology and cognitive impairment in Alzheimer disease: A complex but coherent relationship. *J. Neuropathol. Exp. Neurol.* **68**, 1–14 (2009).
65. Luna-Viramontes, N. I. *et al.* PHF-core tau as the potential initiating event for tau pathology in Alzheimer's disease. *Front. Cell. Neurosci.* **14**, 247 (2020).
66. Shao, C. Y., Mirra, S. S., Sait, H. B. R., Sacktor, T. C. & Sigurdsson, E. M. Postsynaptic degeneration as revealed by PSD-95 reduction occurs after advanced Aβ and tau pathology in transgenic mouse models of Alzheimer's disease. *Acta Neuropathol.* **122**, 285–292 (2011).
67. Liu, J. *et al.* Amyloid-β induces caspase-dependent loss of PSD-95 and synaptophysin through NMDA receptors. *J. Alzheimers. Dis.* **22**, 541–556 (2010).
68. Fitzpatrick, A. W. P. *et al.* Cryo-EM structures of tau filaments from Alzheimer's disease. *Nature* **547**, 185–190 (2017).
69. Yoon, S. *et al.* Drug discovery and screening tool development for tauopathies by focusing on pathogenic tau repeat 3 oligomers. *Angew. Chem. Int. Ed.* **63**, e202411942 (2024).
70. von Bergen, M. *et al.* Assembly of tau protein into Alzheimer paired helical filaments depends on a local sequence motif ((306)VQIVYK(311)) forming beta structure. *Proc. Natl. Acad. Sci.*

U. S. A. **97**, 5129–5134 (2000).

71. Lasagna-Reeves, C. A. *et al.* Tau oligomers impair memory and induce synaptic and mitochondrial dysfunction in wild-type mice. *Mol. Neurodegener.* **6**, 39 (2011).

72. Yang, S. H*. et al*. Nec-1 alleviates cognitive impairment with reduction of Aβ and tau abnormalities in APP/PS 1 mice. *EMBO molecular medicine*. **9** (1) 61-77 (2017)

73. Yang, S. H. *et al*. A small molecule Nec-1 directly induces amyloid clearance in the brains of aged APP/PS1 mice. *Scientific reports*. **9** (1) 4183 (2019)

Acknowledgment

We thank Dr. Dongwook Kim for analyzing the crystal structure of **8a**, and Dr. Kyunghoon Lee for his assistance with the transition state calculations for the [6+4] cycloaddition. This work was supported by the National Research Foundation of Korea (NRF) grant funded by the Korean government (MSIT) (NRF-2021R1A2C2011203, NRF-2018R1A5A1025208, NRF-2021R1A2C2093916, Y.K., RS-2023-00257479) and by the BK21 FOUR Project. This research was supported by Basic Science Research Program through the National Research Foundation of Korea (NRF) funded by the Ministry of Education (2019R1A6A1A10073887). We acknowledge support by Korea Dementia Research Project through the Korea Dementia Research Center (KDRC) (RS-2024-00349158, Y.K.). This research was also supported by KAIST Cross-Generation Collaborative Lab Project.

Author contributions

Seongrok H. synthesized and characterized chemicals. M.C. conducted the full series of pharmacological evaluations from *in vitro* to *in vivo* studies. W.Z. performed the molecular simulation analyses. Seongrok H., M.C., Y.K., and Sunkyu H. wrote the original draft. J.K. participated in 5XFAD long-term drug administration. S.K. assisted in large-scale compound synthesis. J.K. and H.S. were involved in mouse breeding. I.C. and M.P. synthesized fluorescent Aβ peptides. Soljee Y. and W.S. synthesized the R3 peptide. W.S. and Suhyun Y. synthesized $A\beta_{42}$ peptide. J.H. and H.H. carried out the ADME analyses. Seongrok H., M.C., W.Z., W.K., Y.K., and Sunkyu H. analyzed and interpreted the data and wrote the paper. W.K., Y.K., and Sunkyu H. supervised the entire work.

Competing interests

Y.K. is an employee of Amyloid Solution Inc. and received equity or equity options. The remaining authors declare no competing interests.

Fig. 1: Synthesis and biological studies of collinolactone congener 8. a Structures of collinolactone (**1**), collinoketone A (**2**), and collinoketone B (**3**) and characteristics of collinolactone (**1**). **b** Workflow of this study that involves: 1) Chemical synthesis of 3-desoxycollinoketone B (**8**); 2) AI-Assisted molecular simulations of 3-desoxycollinoketone B (**8**) and collinolactone (**1**) with Aβ and tau aggregates; 3) *In vitro* and *in vivo* studies of reduction of aggregates of amyloid-β and tau by 3-desoxycollinoketone B (**8**).

Fig. 2: **Synthesis of the modules. a** Synthesis of module 1. **b** Synthesis of module 2. **c** Synthesis of module 3.

Fig. 3: Synthesis of 3-desoxy-collinoketone B (8a).

Fig. 4: Calculation-assisted mechanistic investigations of the key transannular cycloaddition reaction computed with SMD(toluene)-M06-2X/6-311+G(d,p)//M06-2X/6-31G(d,p).

Fig. 5: AI-assisted molecular modeling and simulation of 3-desoxy-collinoketone B (8a) and collinolactone (1) on $A\beta_{42}$ and Tau aggregates. a The overview of a workflow involving binding pose prediction followed by disaggregation simulation. **b** The representative predicted pose of 3-desoxy-collinoketone B (**8a**) binding to $A\beta_{42}$ fibril, and **c** its interaction profile analyzed with PLIP software. **d** The representative predicted pose of 3-desoxy-collinoketone B (**8a**) binding to Tau fibril, and **e** its interaction profile analyzed with PLIP. Bars and numbers within the plots represent the mean values and sample sizes of predicted binding free energies of the poses sampled from **f** DiffDock-L and **g** NeuralPLexer2, respectively. Error bars indicate the 95% confidence interval. Statistical significance was determined using one-tailed unpaired *t*-tests, with *P* values indicated by asterisks. (***P* < 0.01, ****P* < 0.001, and *****P* < 0.0001) **h** The Cα root-mean-square fluctuation (RMSF) profiles of the $A\beta_{42}$ fibril in the presence and absence of 3-desoxy-collinoketone B (**8a**), along with the corresponding fibril structure highlighting the **8a**-induced highly flexible region in blue. **i** Illustration of the progressive disruption of the $A\beta_{42}$ fibril upon the binding of 3-desoxy-collinoketone B (**8a**) during the 100 ns MD simulation. Source data are provided as a Source Data file.

Fig. 6: Therapeutic effect of 3-desoxy-collinoketone B (8a) on Aβ aggregates. a Thioflavin-T (ThT) assay results demonstrating the inhibitory effect of 3-desoxy-collinoketone B (**8a**) on $A\beta_{42}$ aggregation. **b** ThT assay results on the dissociative effects of 3-desoxy-collinoketone B (**8a**) against pre-formed $A\beta_{42}$ fibrils. **c** Amyloid aggregate assay (A3) based efficacy test utilized to

evaluate the dissociation percentage resulting from 3-desoxy-collinoketone B (**8a**) on $A\beta_{42}$ oligomers. **d** PAMPA-BBB assay to evaluate BBB permeability. **e** *In vivo* therapeutic efficacy test utilizing 5XFAD mouse model (APP and PSEN1 mutation): ThS-stained fluorescence half-brain images of vehicle and 3-desoxy-collinoketone B (**8a**) 5-daily administered group. **f** Quantification of Aβ plaques in cortical regions of ThS-stained brains, and quantification of total Aβ (6E10) and oligomeric Aβ (A11) in RIPA-soluble lysates of cortex. **g** Quantification of Aβ plaques in hippocampal regions of ThS-stained brains, and quantification of total Aβ (6E10) and oligomeric Aβ (A11) in RIPA-soluble lysates of the hippocampus. **j** *In vivo* therapeutic efficacy test utilizing 5XFAD mouse model (APP and PSEN1 mutation): ThS-stained fluorescence half-brain images of vehicle and 3-desoxy-collinoketone B (**8a**) one month administered group. **k** Quantification of Aβ plaques in cortical regions of ThS-stained brains, and **l** quantification of total Aβ (6E10) and oligomeric Aβ (A11) in RIPA-soluble lysates of cortex. **m** Quantification of Aβ plaques in hippocampal regions of ThS-stained brains, and **n** quantification of total Aβ (6E10) and oligomeric Aβ (A11) in RIPA-soluble lysates of the hippocampus. Data are presented as mean ± SEM. For ThT assay, data were derived from n = 3 technical replicates and analyzed using one-way ANOVA. Plaque counting data were obtained from n = 3 biological replicates for 5-day administration and n = 4 biological replicates for 4-week administration and analyzed using two-tailed unpaired *t*-test. Bonferroni's post hoc correction was applied for multiple comparisons in all statistical analyses (*$P < 0.05$, ***$P < 0.001$, ****$P < 0.0001$, and other comparisons not significant). Source data are provided as a Source Data file. Abbreviations: Aβ aggr. = Aβ aggregation; Cpd. = Compound; TG = Transgenic; IB = Immunoblotting

Fig. 7: Therapeutic effect of 3-desoxy-collinoketone B (8a) on tau aggregates. a Tau protein consists of four domains: N-terminal, proline rich region, repeat domain (R1-R4), and C-terminal domain. **b** ThT assay results demonstrating the inhibitory effect of 3-desoxy-collinoketone B (**8a**) on tau K18 aggregation. **c** ThT assay results on the dissociative effects of 3-desoxy-collinoketone B (**8a**) against pre-formed tau K18 aggregates. **d** 3-desoxy-collinoketone B (**8a**) therapeutic efficacy test *in vivo* utilizing PS19 mouse model (MAPT P301S mutation): Expression levels of postsynaptic density protein 95 (PSD95) and synaptophysin in the hippocampus region of PS19 mice brain. **e** ThT assay results dcting the inhibitory effect of 3-desoxy-collinoketone B (**8a**) on R3 aggregation. **f** ThT assay results showing the dissociative effects of 3-desoxy-collinoketone B (**8a**) against pre-formed R3 aggregates. **g** 3-desoxy-collinoketone B (**8a**) therapeutic efficacy test *in vivo* utilizing R3-infused acute AD mouse model: Dot blot assay to visualize R3 oligomer amounts in injected samples. **h** The overall experimental scheme of Y-maze test, and the percentage of

spontaneous alternation and the count of arm entry. **i** Novel object recognition (NOR) exploration time and discrimination index. Data are presented as mean ± SEM. ThT assay data were derived from n = 3 technical replicates and analyzed using one-way ANOVA. Western blot data were obtained from n = 4 biological replicates and analyzed using one-way ANOVA. Y-maze data were obtained from n = 9 biological replicates and analyzed using one-way ANOVA. NOR data were obtained from n = 10 biological replicates and analyzed using two-tailed unpaired *t*-test for exploration time and one-way ANOVA for discrimination index. Bonferroni's post hc correction was applied for multiple comparisons in all statistical analyses (*P < 0.05, ***P < 0.001, ****P < 0.0001, and other comparisons not significant). Source data are provided as a Source Data file. Abbreviations: aggr. = aggregation; Cpd. = Compound; WT = Wild-type; TG = Transgenic; IB = Immunoblotting; Veh = Vehicle

Table. 1: ADME assay of 3-desoxy-collinoketone B (**8a**)

			8a	reference
Plasma Assay[a]	**Human**		101.75	0.03[c]
	Mouse		105.8	3.13[c]
Microsomal Stability Assay[a]	**Human**		7.12	12.00[d]
	Mouse		6.15	2.66[d]
CYP450 Inhibition Assay[b]	**1A2**		116.43	45.29[e]
	2B6		114.2	117.09[e]
	2C8		121.16	101.32[e]
	2C9		102.19	105.17[e]
	2C19		55.54	84.93[e]
	2D6		87.71	95.28[e]
	3A4	(Mida)	112.97	7.20[f]
		(Test)	80.91	2.94[f]

[a]Results were expressed as % remaining. [b]Results were expressed as % activity. [c]Reference Procaine (10 μM). [d]Verapamil (1 μM). [e]Furafyllin (5 μM). [f]Ketoconazole (1 μM)

Editorial Summary:
This study describes the synthesis of 3-desoxy-collinoketone B, a small molecule that targets amyloid-β and tau aggregates. In mouse models, it crosses the blood-brain barrier, reduces plaques, and ameliorates learning and memory impairments.

Peer review information: *Nature Communications* thanks the anonymous reviewers for their contribution to the peer review of this work. A peer review file is available.

a

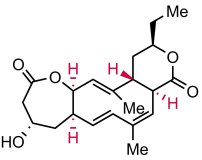

collinolactone (**1**, rhizolutin, ref 6, 7, 8, and 23)

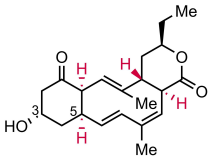

collinoketone A (**2**, ref 8, 9 and 10)

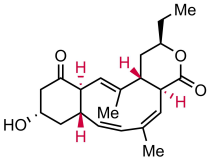

collinoketone B (**3**, ref 8, 9 and 10)

- Unprecedented 7/10/6 tricyclic bislactone.
- Disaggregation of both Aβ plaques and tau tangles.

- Revised structure of rhizolutin.
- Low isolation yield from natural sources.
- Not accessible to cortex.

b

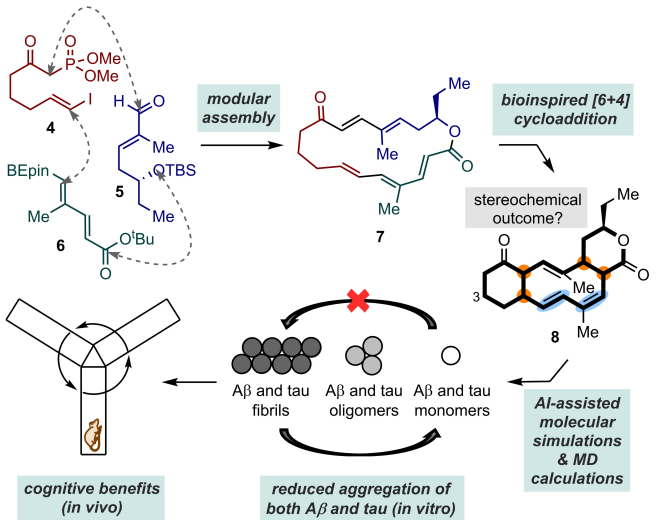

a

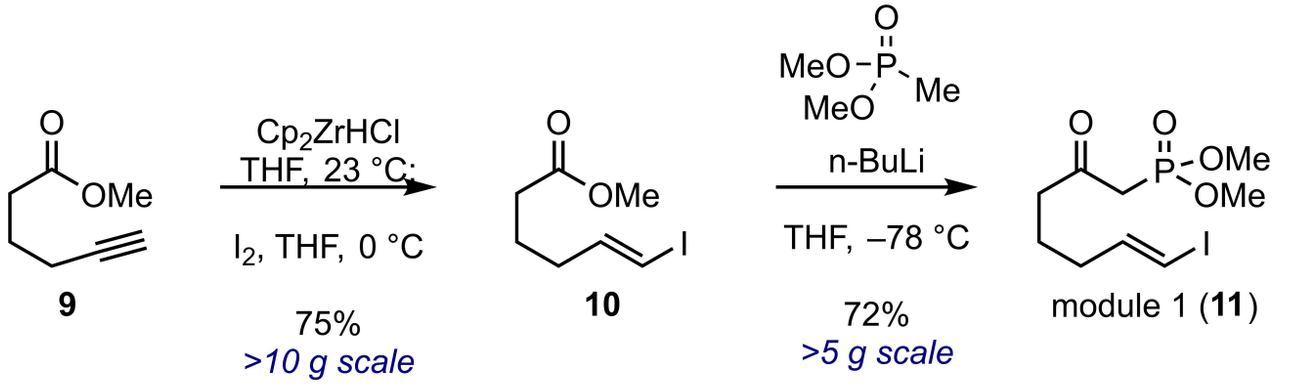

b

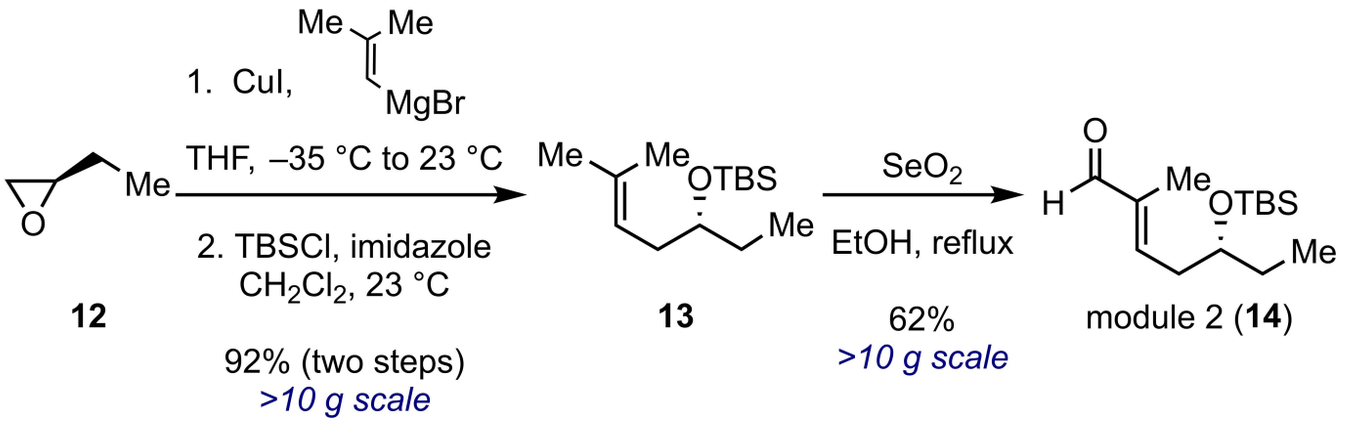

c

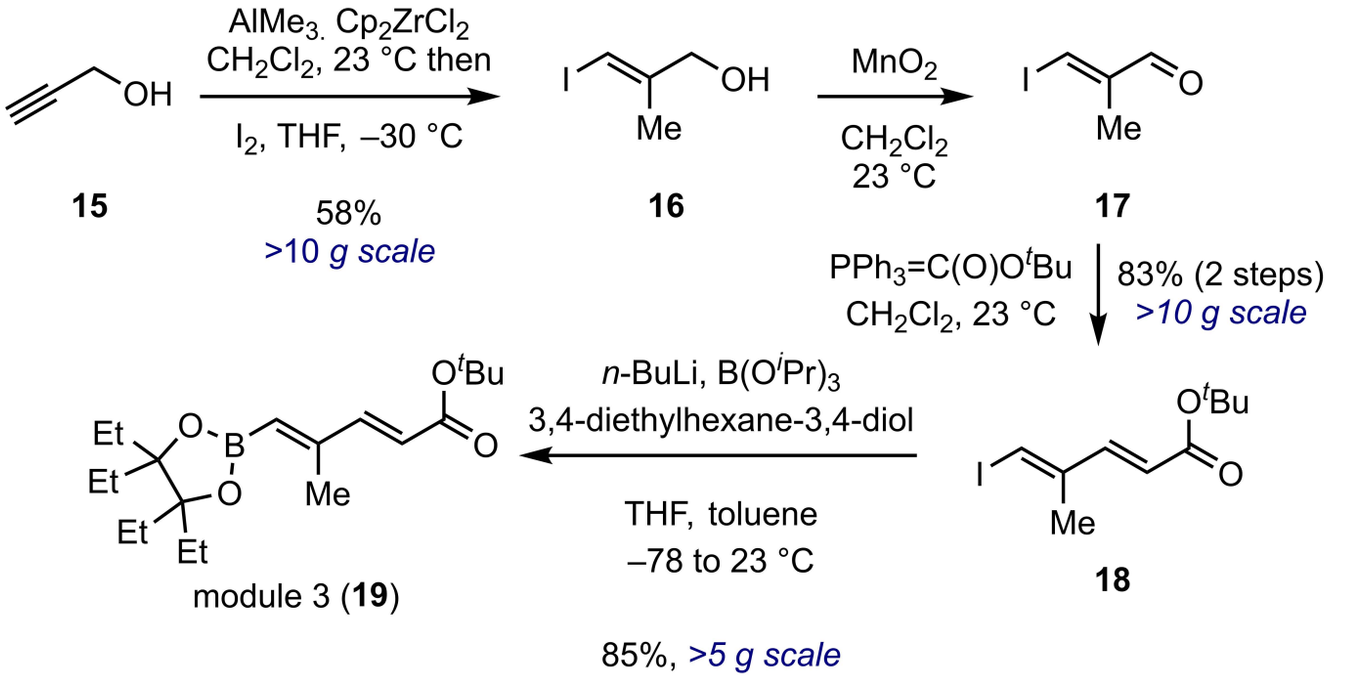

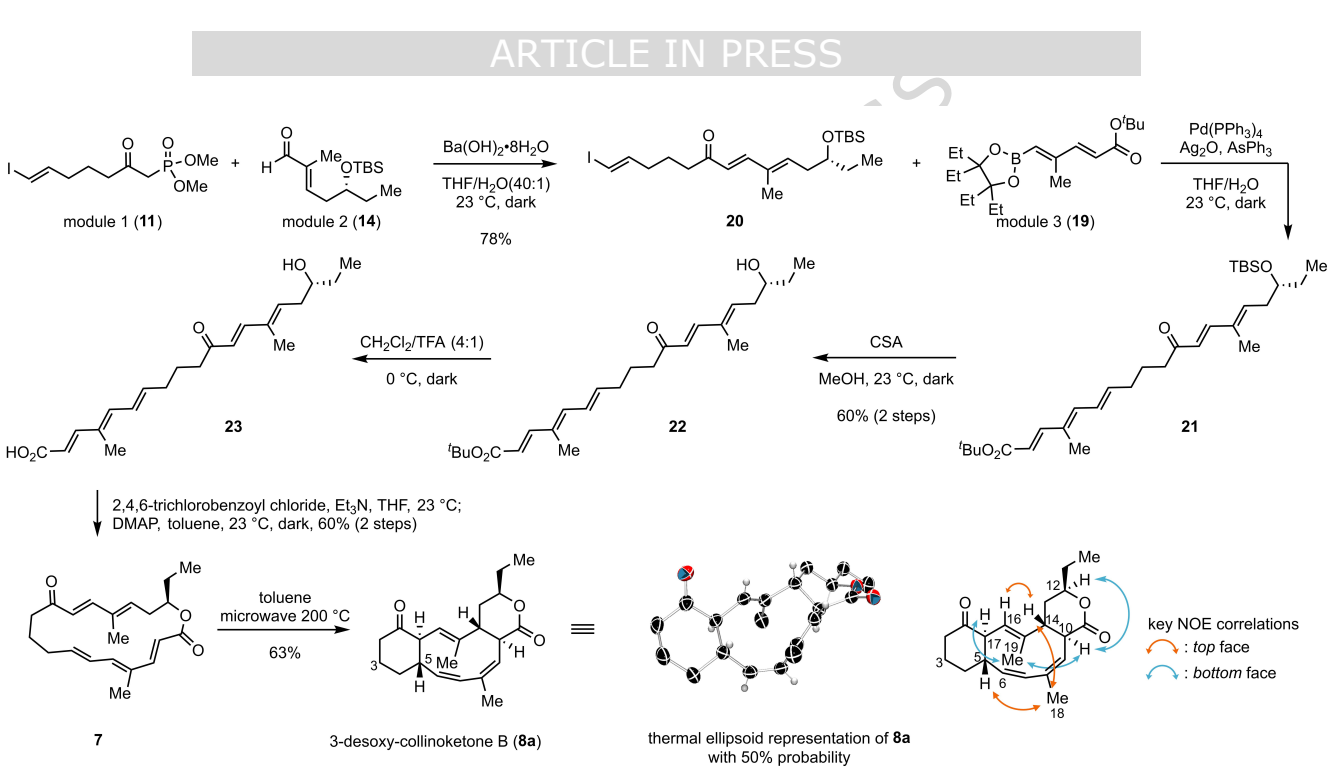
module 1 (11)
module 2 (14)
Ba(OH)2•8H2O
THF/H2O(40:1)
23 °C, dark
78%
20
module 3 (19)
Pd(PPh3)4
Ag2O, AsPh3
THF/H2O
23 °C, dark
21
CSA
MeOH, 23 °C, dark
60% (2 steps)
22
CH2Cl2/TFA (4:1)
0 °C, dark
23
2,4,6-trichlorobenzoyl chloride, Et3N, THF, 23 °C;
DMAP, toluene, 23 °C, dark, 60% (2 steps)
7
toluene
microwave 200 °C
63%
3-desoxy-collinoketone B (8a)
thermal ellipsoid representation of 8a
with 50% probability
key NOE correlations
: top face
: bottom face

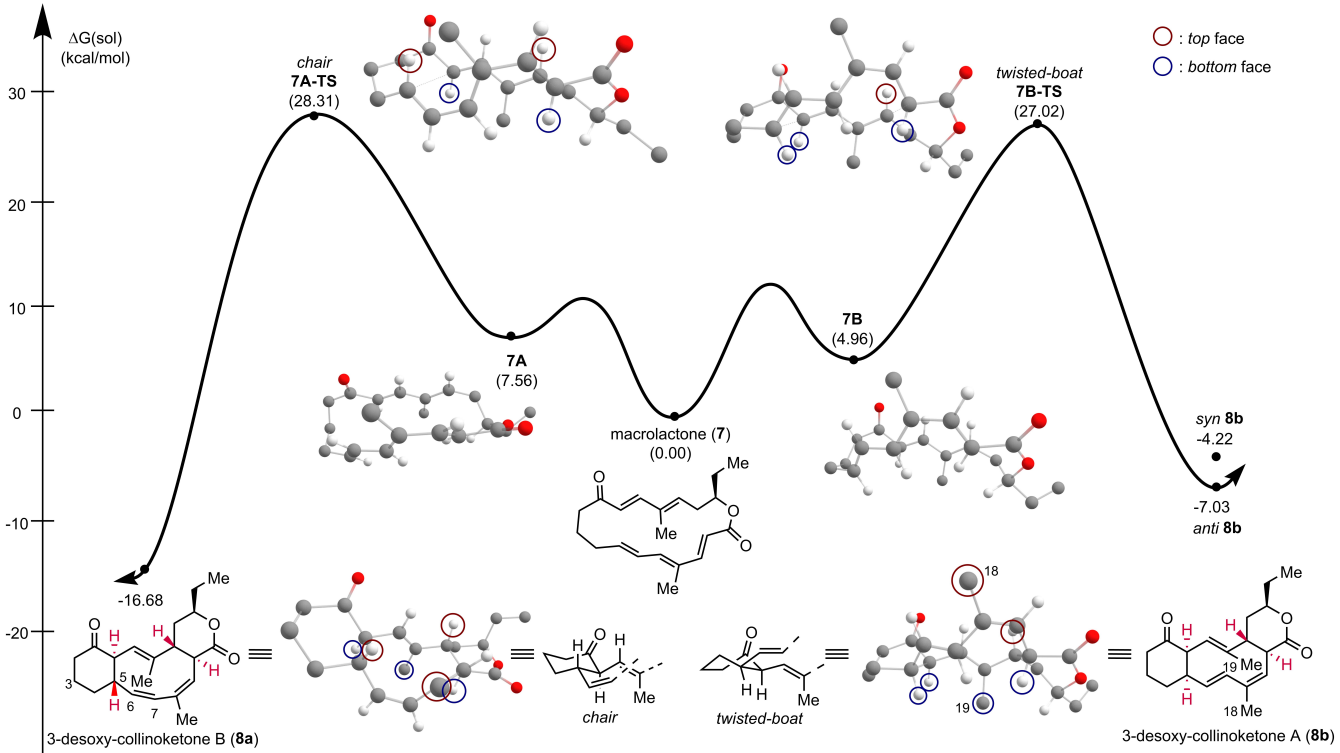
ΔG(sol)
(kcal/mol)
30
20
10
0
-10
-20
chair
7A-TS
(28.31)
twisted-boat
7B-TS
(27.02)
: top face
: bottom face
7A
(7.56)
7B
(4.96)
macrolactone (7)
(0.00)
syn 8b
-4.22
-7.03
anti 8b
-16.68
3-desoxy-collinoketone B (8a)
chair
twisted-boat
3-desoxy-collinoketone A (8b)

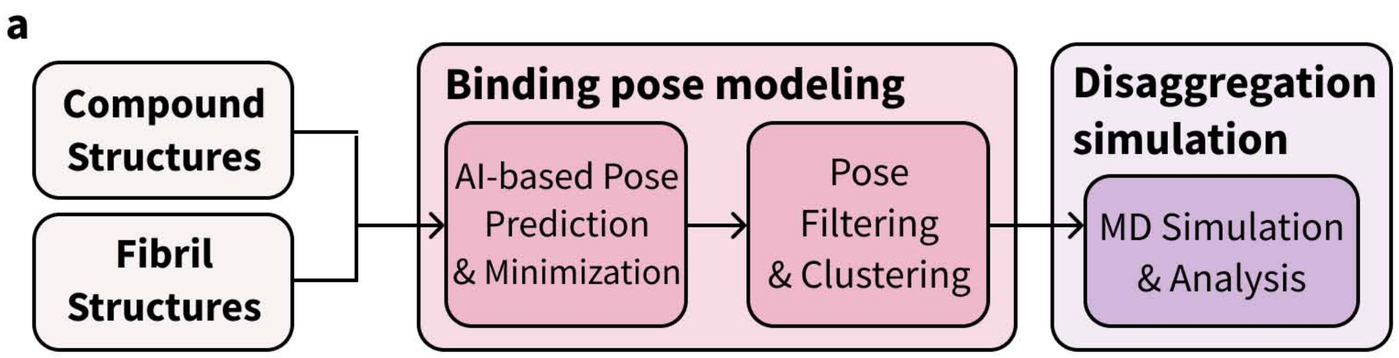
a
Compound Structures
Fibril Structures
Binding pose modeling
AI-based Pose Prediction & Minimization
Pose Filtering & Clustering
Disaggregation simulation
MD Simulation & Analysis

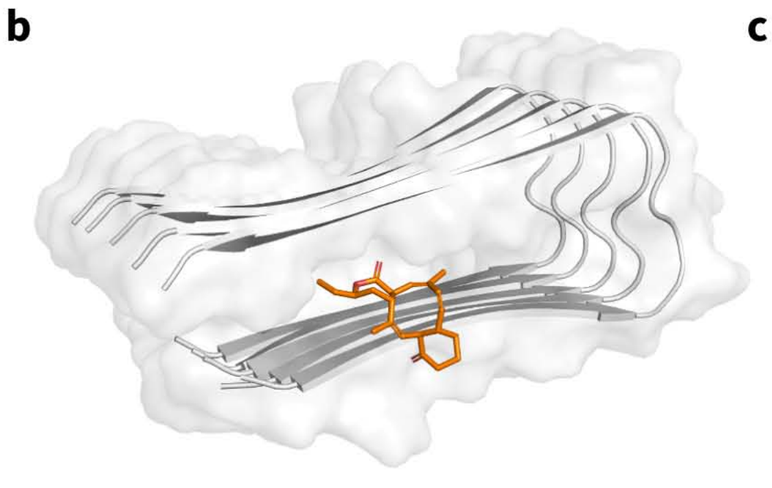
b

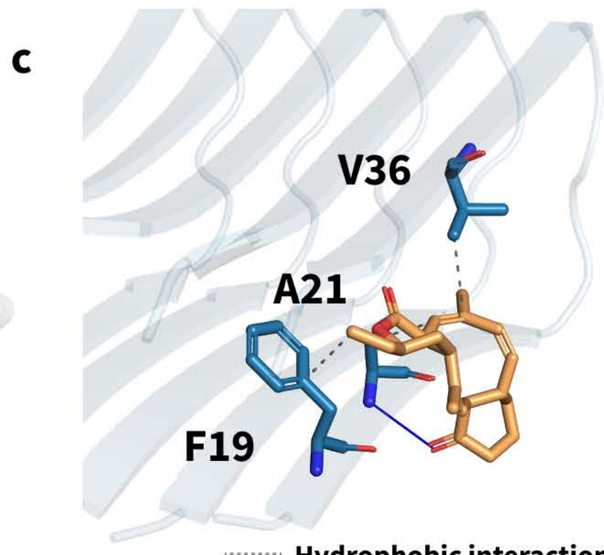
c
V36
A21
F19

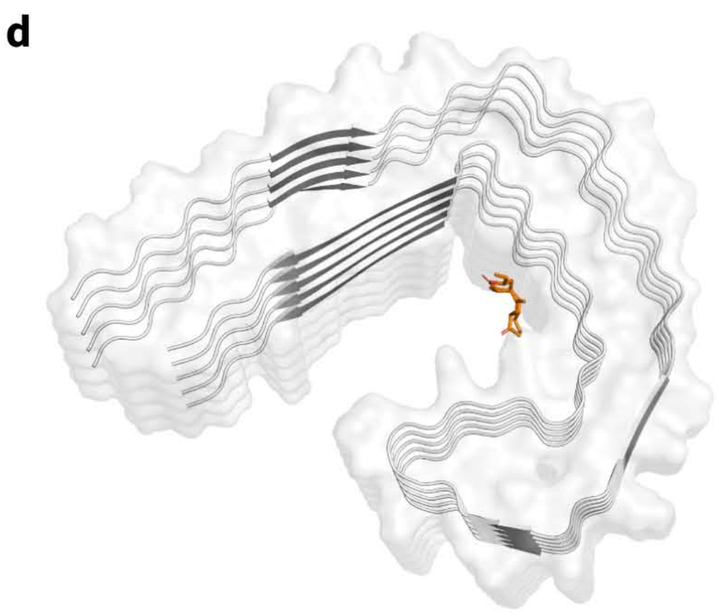
d

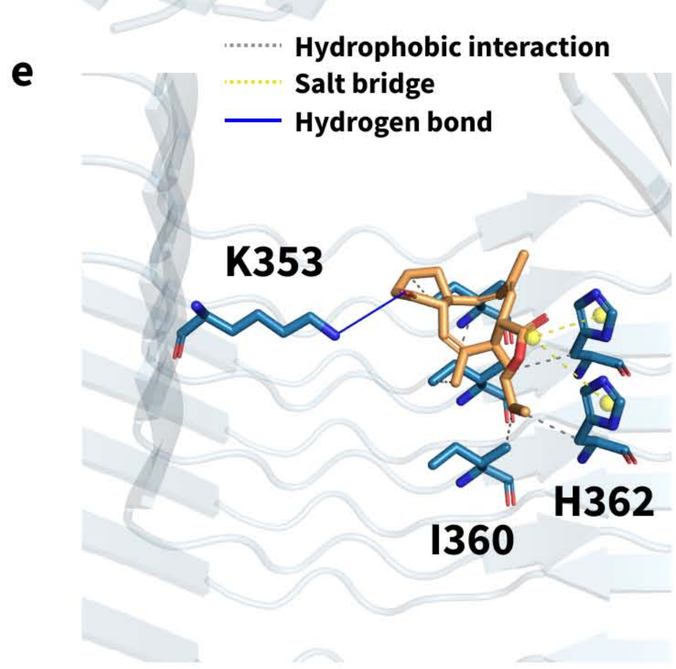
e
Hydrophobic interaction
Salt bridge
Hydrogen bond
K353
H362
I360

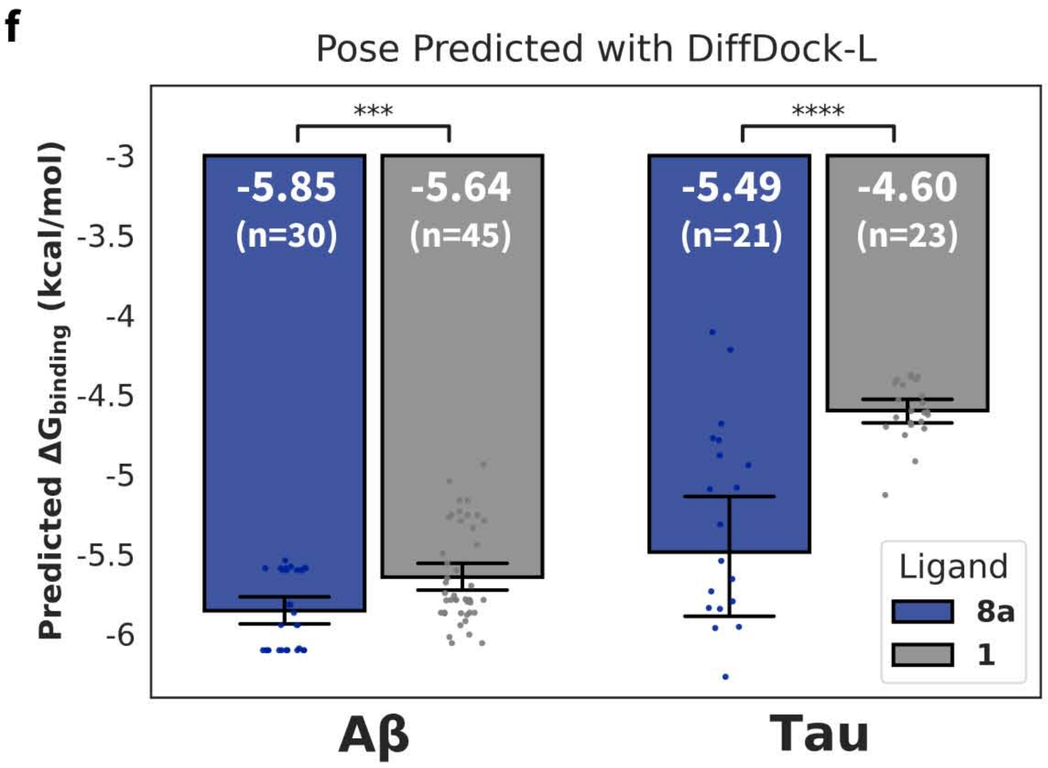
f
Pose Predicted with DiffDock-L
Predicted ΔG_binding (kcal/mol)
-3
-3.5
-4
-4.5
-5
-5.5
-6
***
****
-5.85 (n=30)
-5.64 (n=45)
-5.49 (n=21)
-4.60 (n=23)
Ligand
8a
1
Aβ
Tau

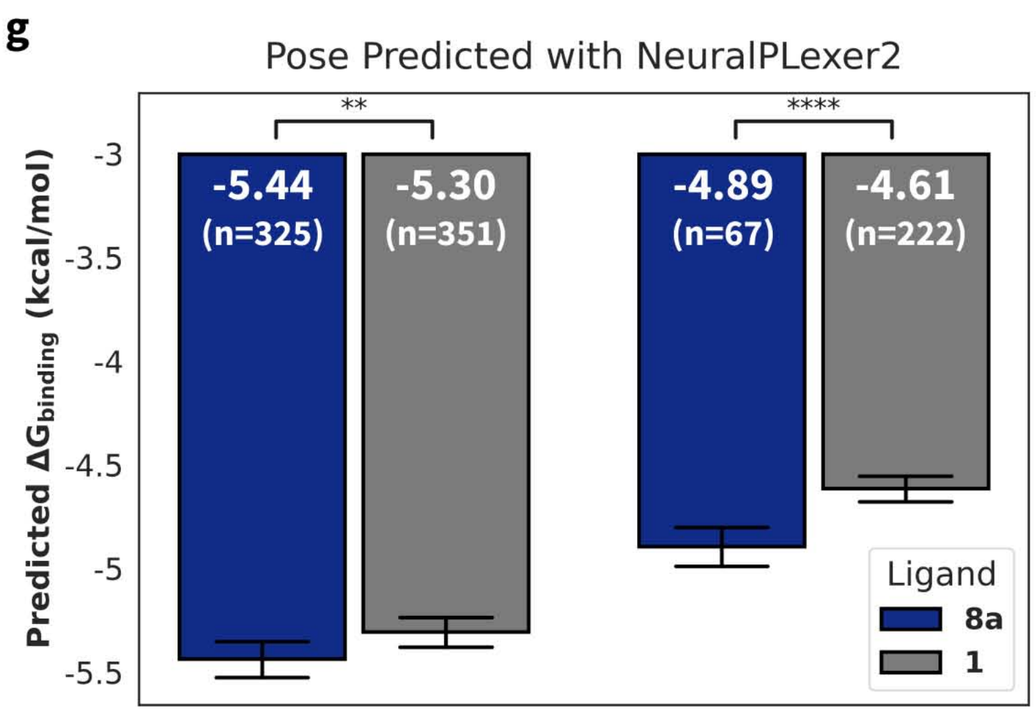
g
Pose Predicted with NeuralPLexer2
Predicted ΔG_binding (kcal/mol)
-3
-3.5
-4
-4.5
-5
-5.5
**
****
-5.44 (n=325)
-5.30 (n=351)
-4.89 (n=67)
-4.61 (n=222)
Ligand
8a
1
Aβ
Tau

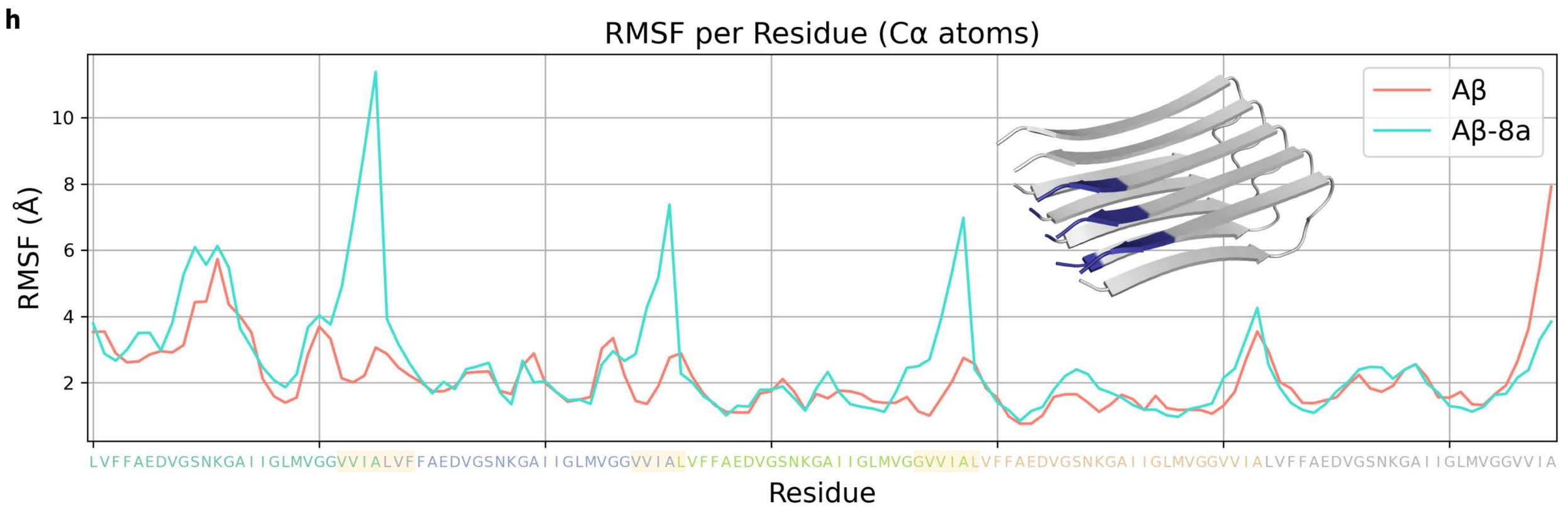
h
RMSF per Residue (Cα atoms)
RMSF (Å)
10
8
6
4
2
Aβ
Aβ-8a
LVFFAEDVGSNKGAIIGLMVGGVVIALVFFAEDVGSNKGAIIGLMVGGVVIALVFFAEDVGSNKGAIIGLMVGGVVIALVFFAEDVGSNKGAIIGLMVGGVVIA
Residue

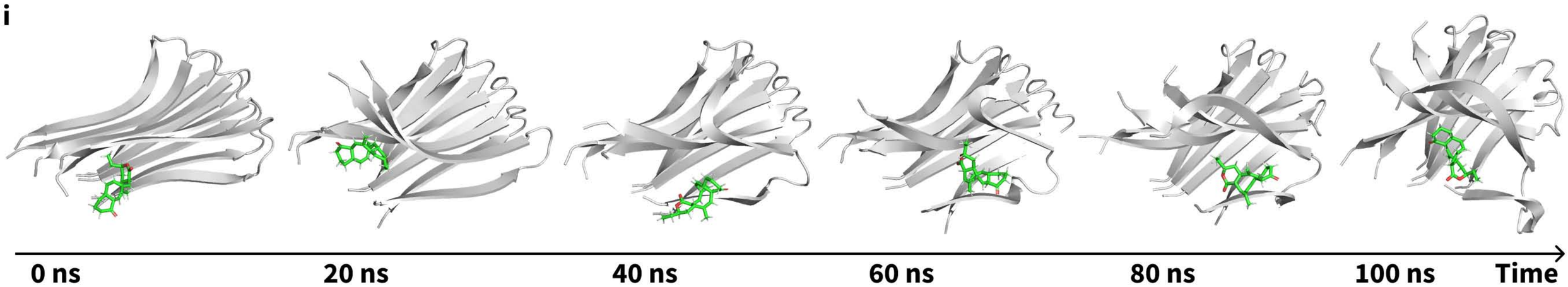
i
0 ns
20 ns
40 ns
60 ns
80 ns
100 ns
Time

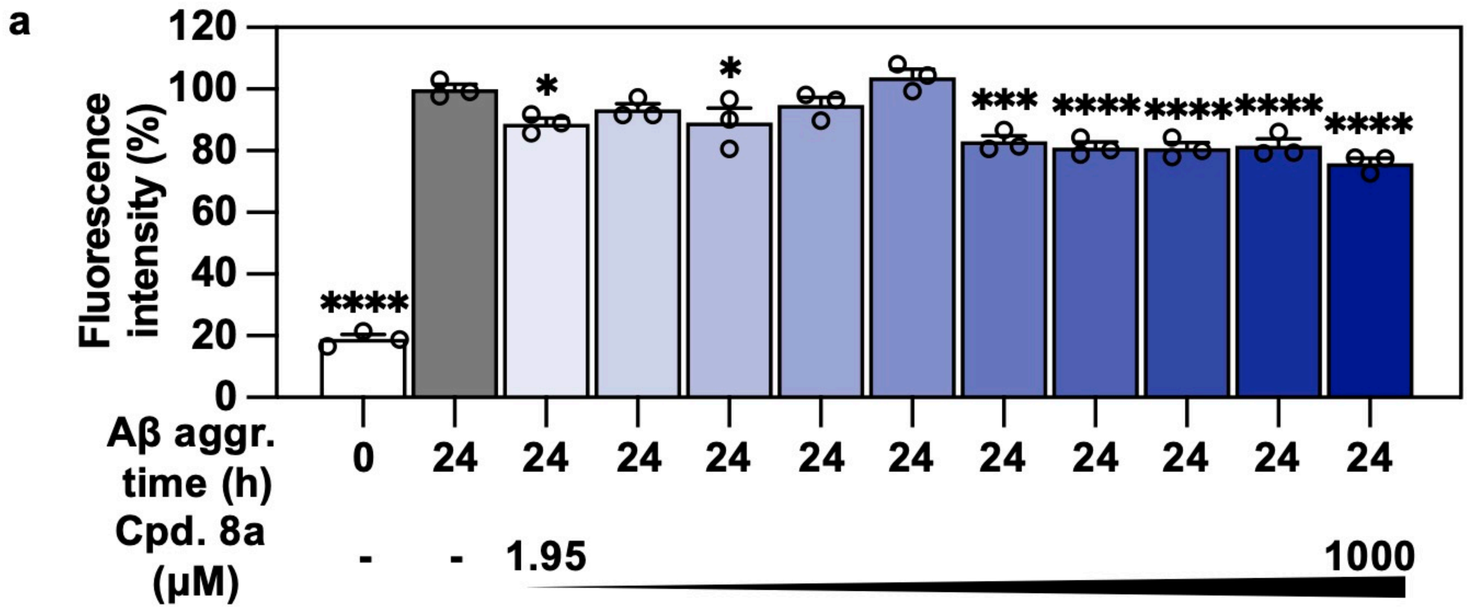
a
Fluorescence intensity (%)
Aβ aggr. time (h)
Cpd. 8a (μM)
0 24 24 24 24 24 24 24 24 24 24 24
- - 1.95 1000

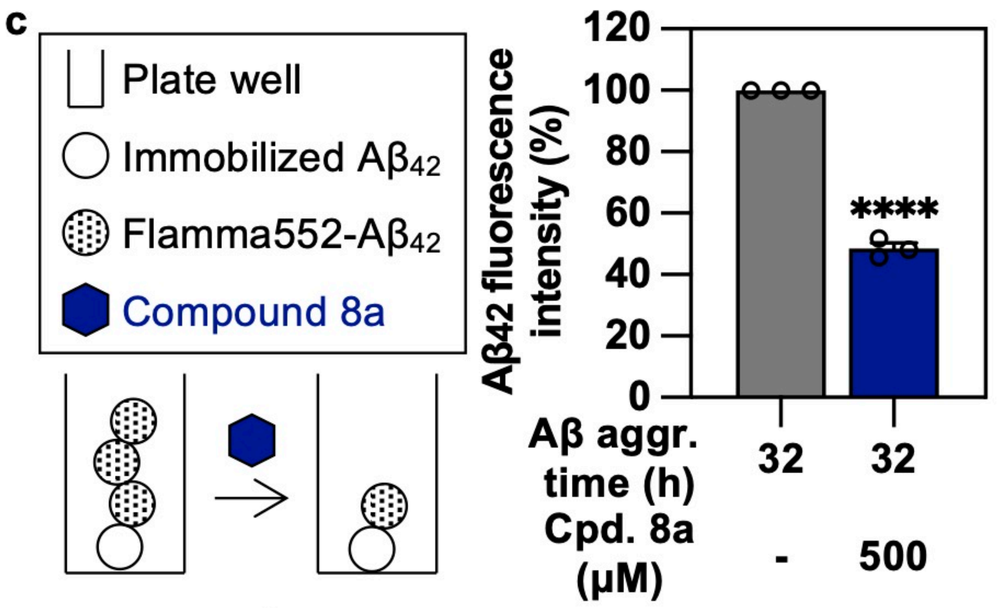
c
Plate well
Immobilized Aβ42
Flamma552-Aβ42
Compound 8a
Aβ42 fluorescence intensity (%)
Aβ aggr. time (h)
Cpd. 8a (μM)
32 32
- 500

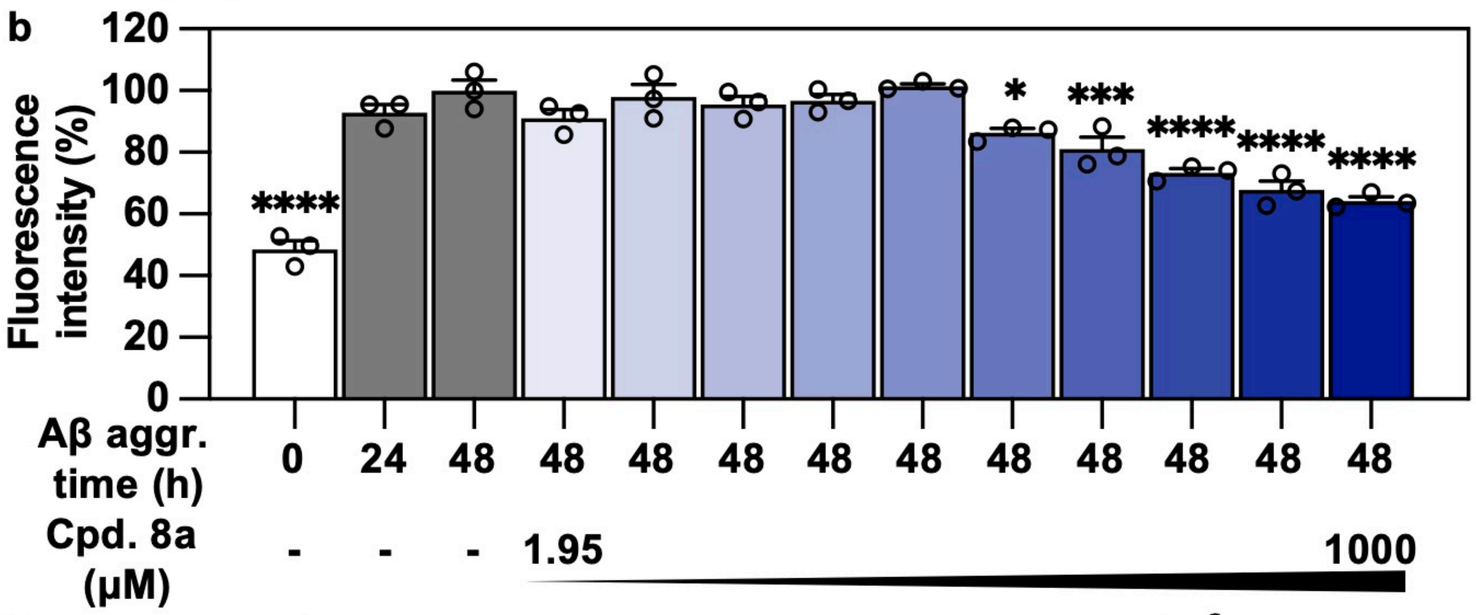
b
Fluorescence intensity (%)
Aβ aggr. time (h)
Cpd. 8a (μM)
0 24 48 48 48 48 48 48 48 48 48 48 48
- - - 1.95 1000

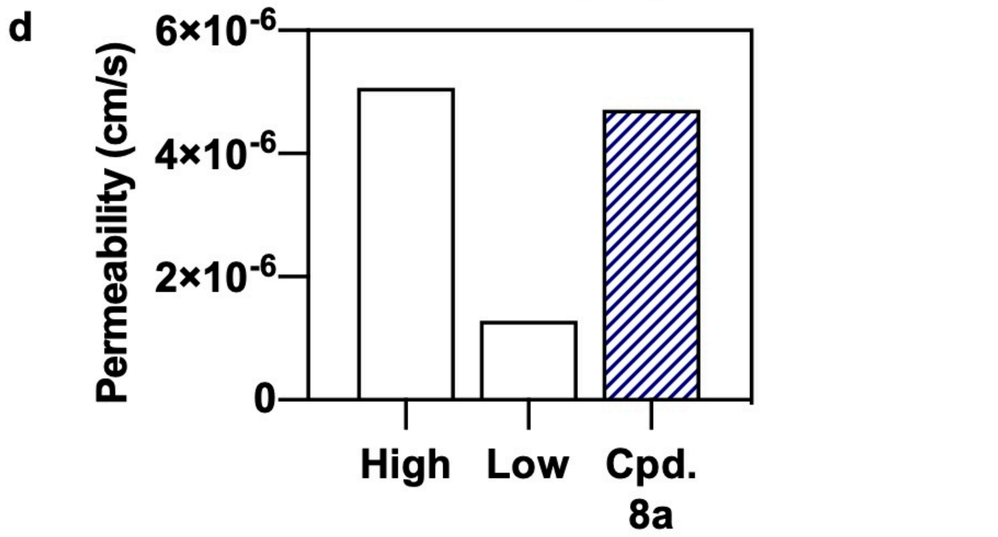
d
Permeability (cm/s)
High Low Cpd. 8a

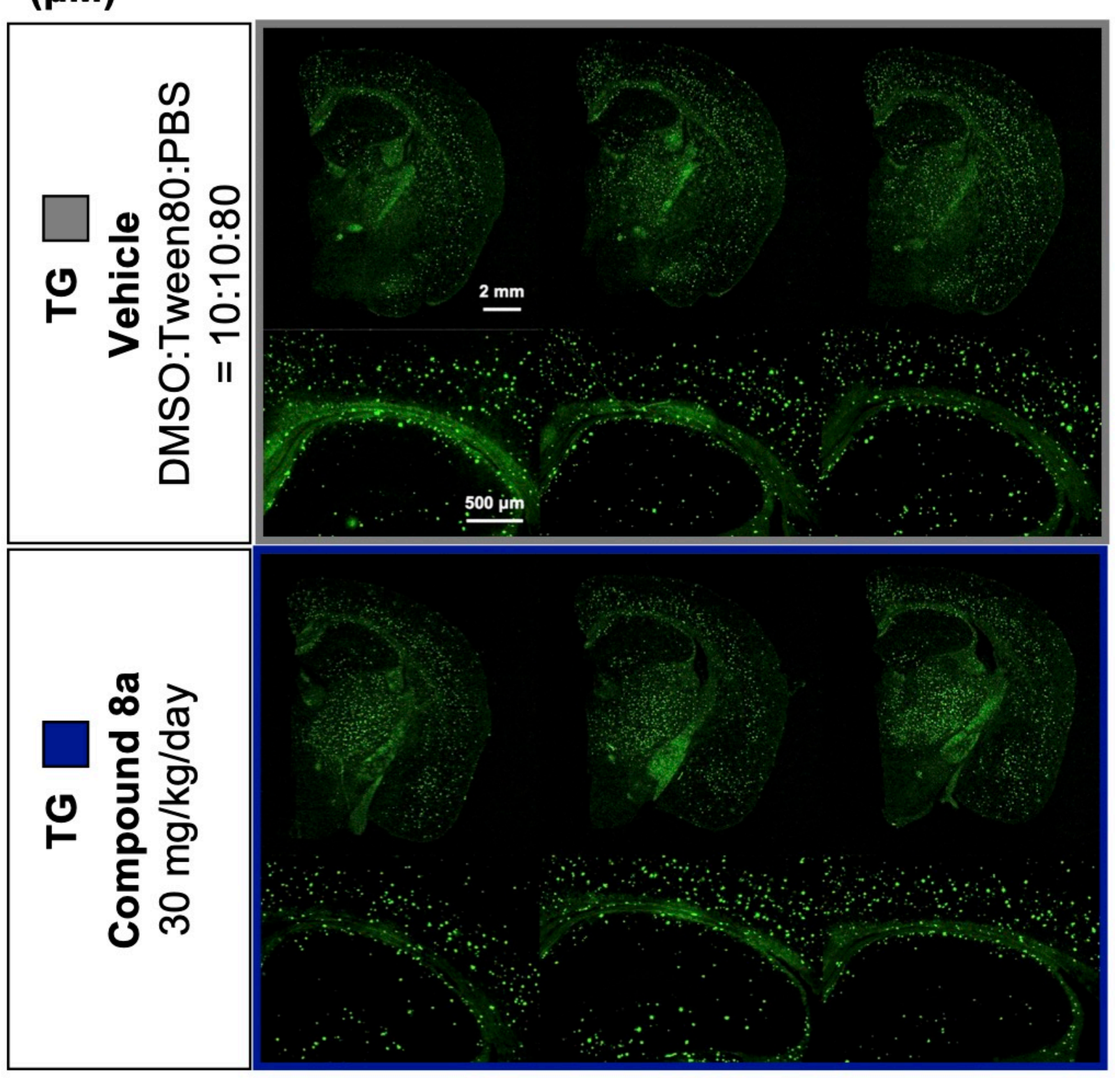
e
TG
Vehicle
DMSO:Tween80:PBS = 10:10:80
2 mm
500 μm
TG
Compound 8a
30 mg/kg/day

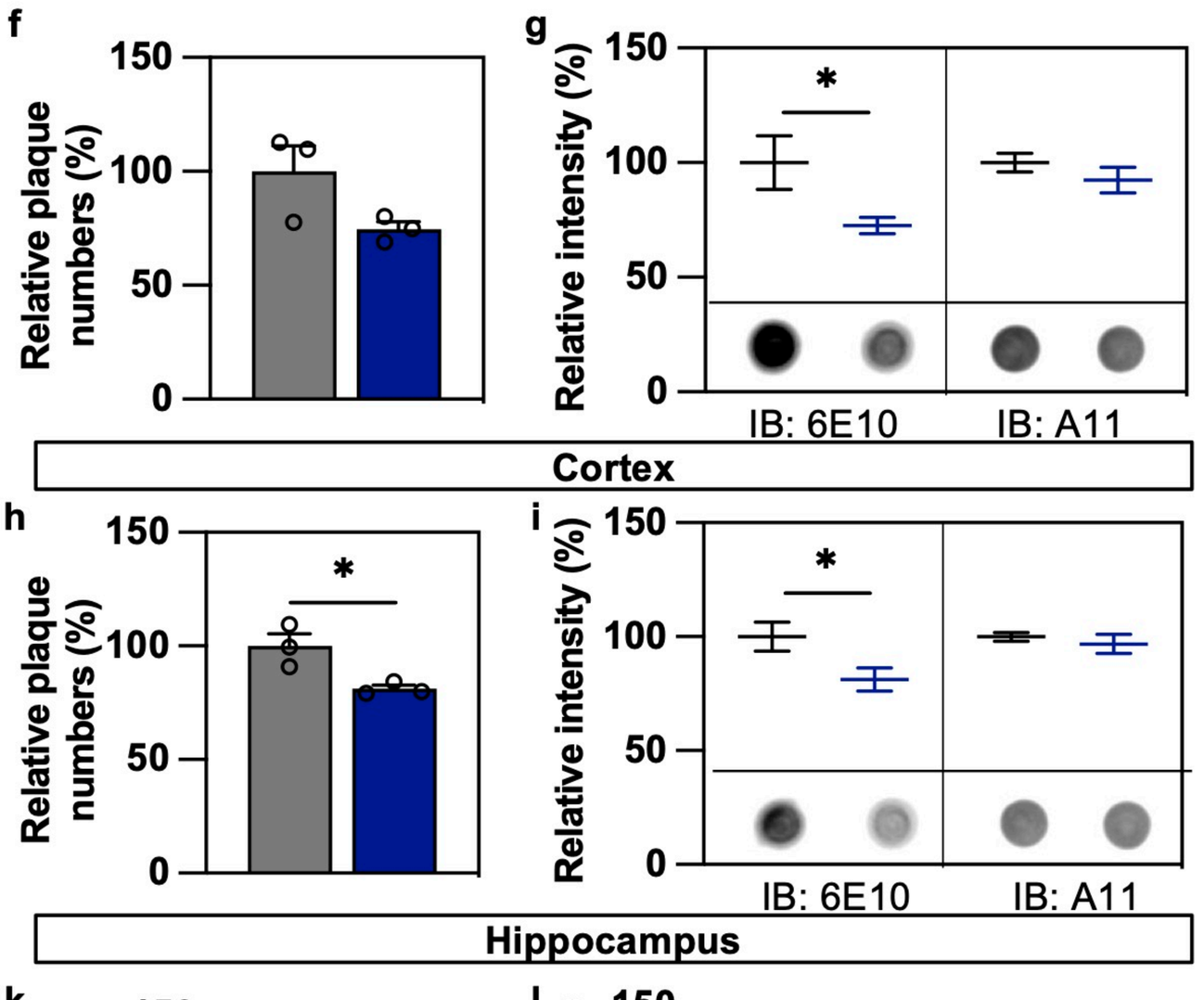
f
Relative plaque numbers (%)
g
Relative intensity (%)
IB: 6E10
IB: A11
Cortex
h
Relative plaque numbers (%)
i
Relative intensity (%)
IB: 6E10
IB: A11
Hippocampus

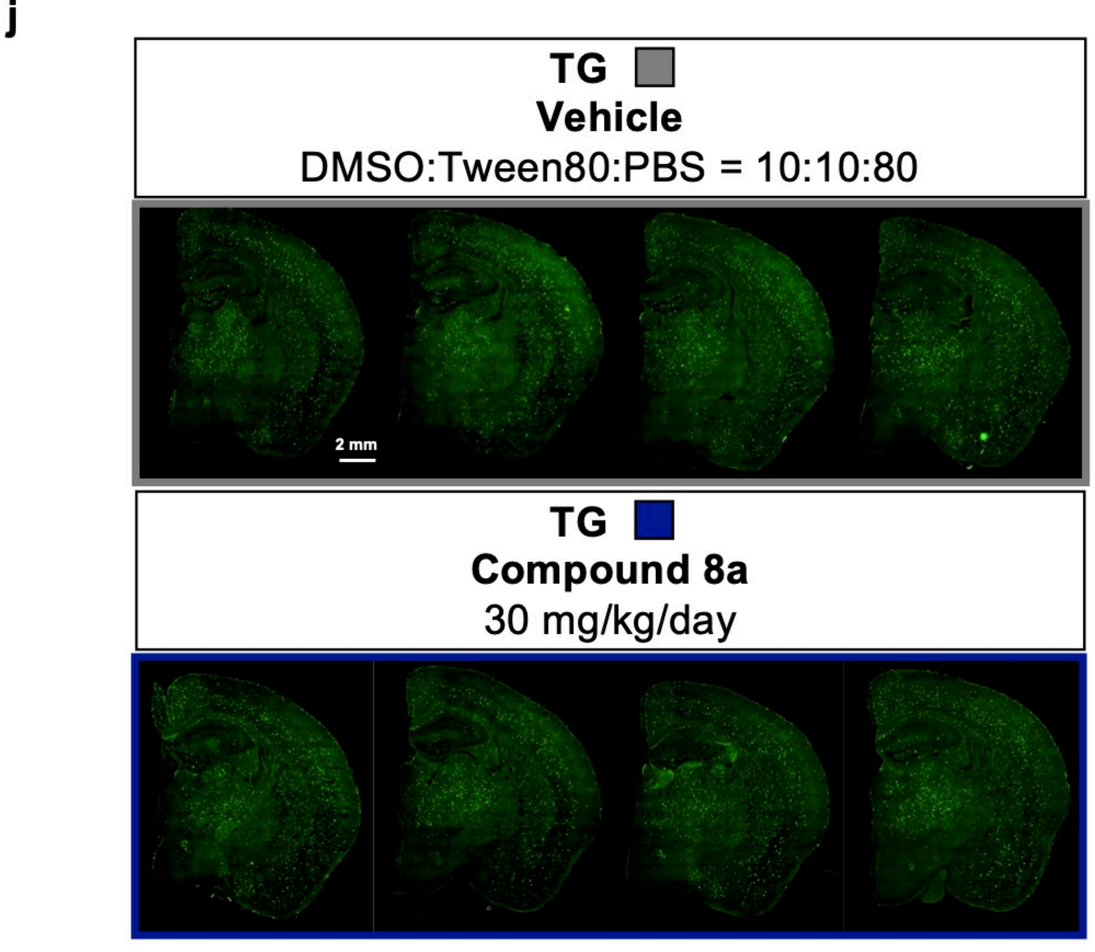
j
TG
Vehicle
DMSO:Tween80:PBS = 10:10:80
2 mm
TG
Compound 8a
30 mg/kg/day

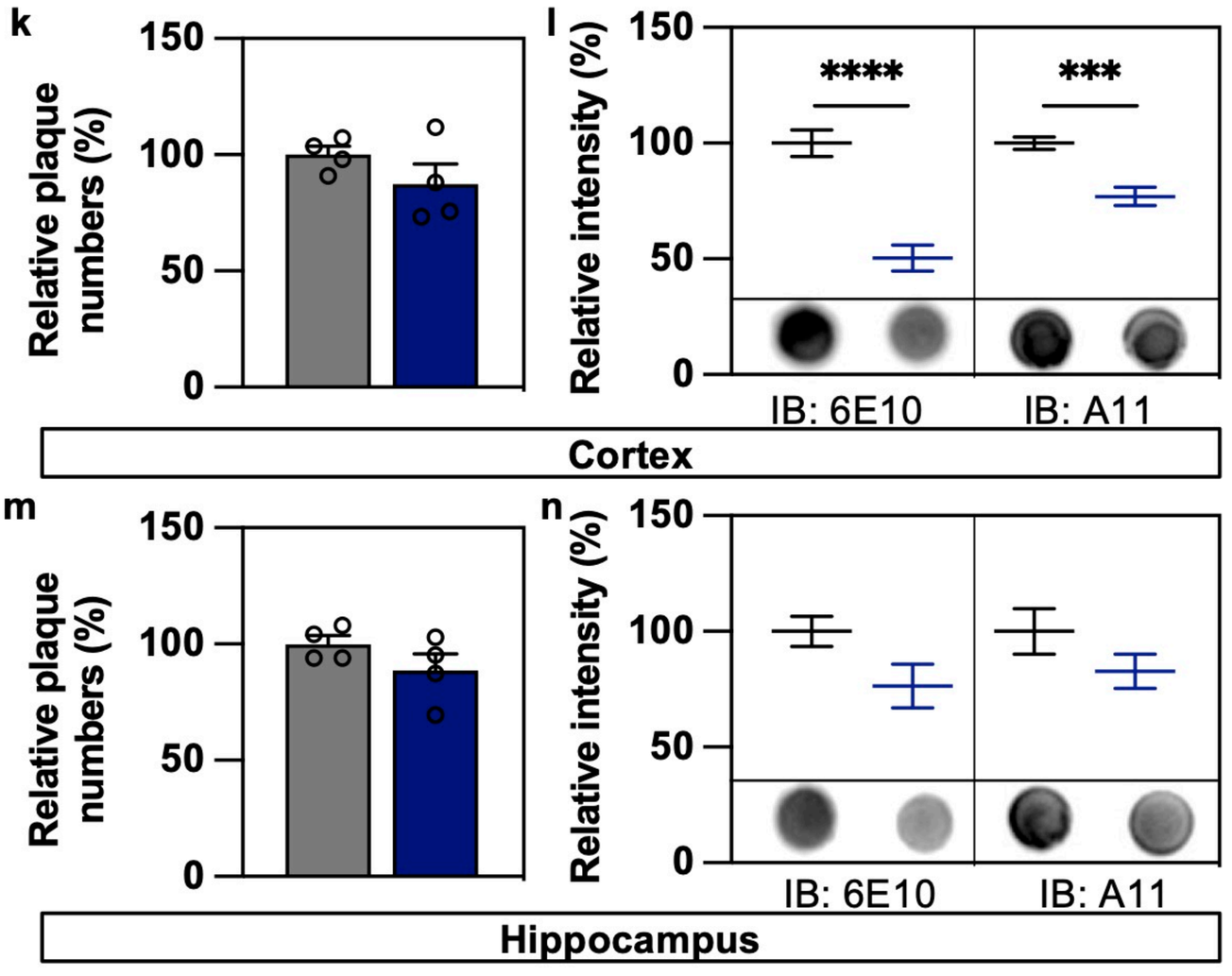
k
Relative plaque numbers (%)
l
Relative intensity (%)
IB: 6E10
IB: A11
Cortex
m
Relative plaque numbers (%)
n
Relative intensity (%)
IB: 6E10
IB: A11
Hippocampus

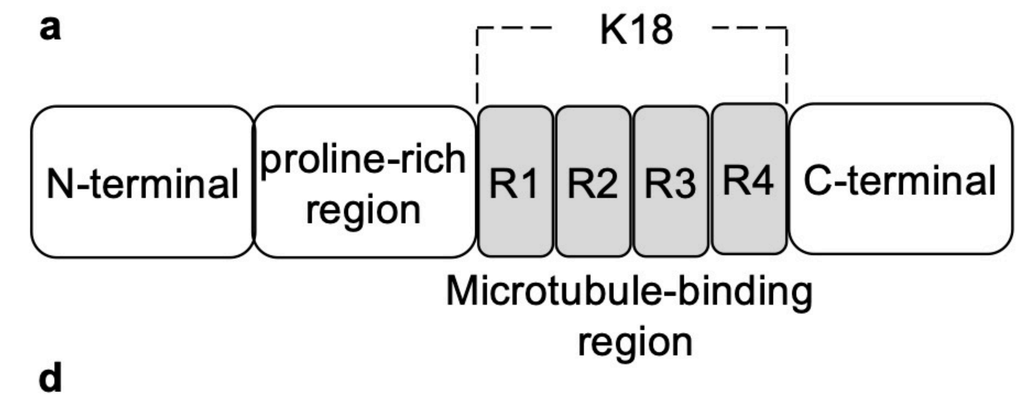
a
K18
N-terminal
proline-rich region
R1
R2
R3
R4
C-terminal
Microtubule-binding region

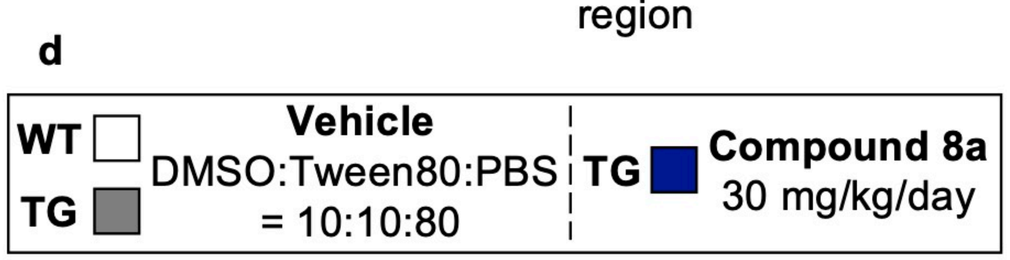
d
WT
TG
Vehicle
DMSO:Tween80:PBS = 10:10:80
TG
Compound 8a
30 mg/kg/day

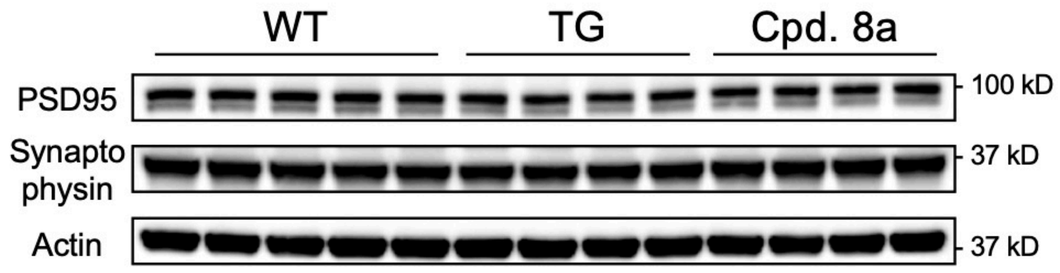
WT
TG
Cpd. 8a
PSD95
100 kD
Synapto physin
37 kD
Actin
37 kD

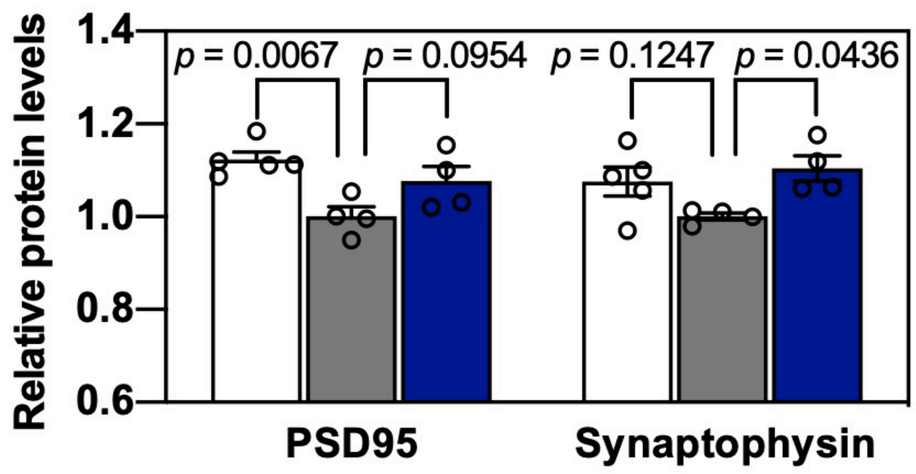
Relative protein levels
1.4
1.2
1.0
0.8
0.6
p = 0.0067
p = 0.0954
p = 0.1247
p = 0.0436
PSD95
Synaptophysin

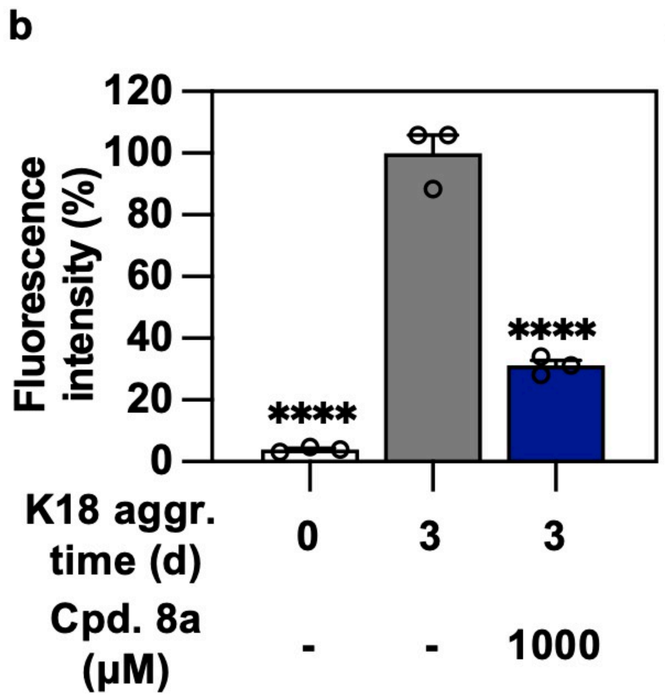
b
Fluorescence intensity (%)
120
100
80
60
40
20
0
****
****
K18 aggr. time (d)
0
3
3
Cpd. 8a (μM)
-
-
1000

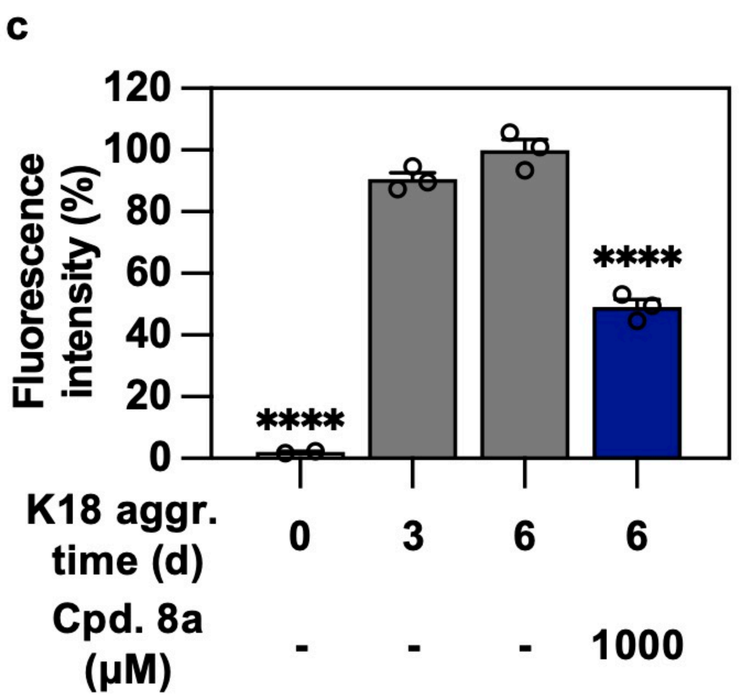
c
Fluorescence intensity (%)
120
100
80
60
40
20
0
****
****
K18 aggr. time (d)
0
3
6
6
Cpd. 8a (μM)
-
-
-
1000

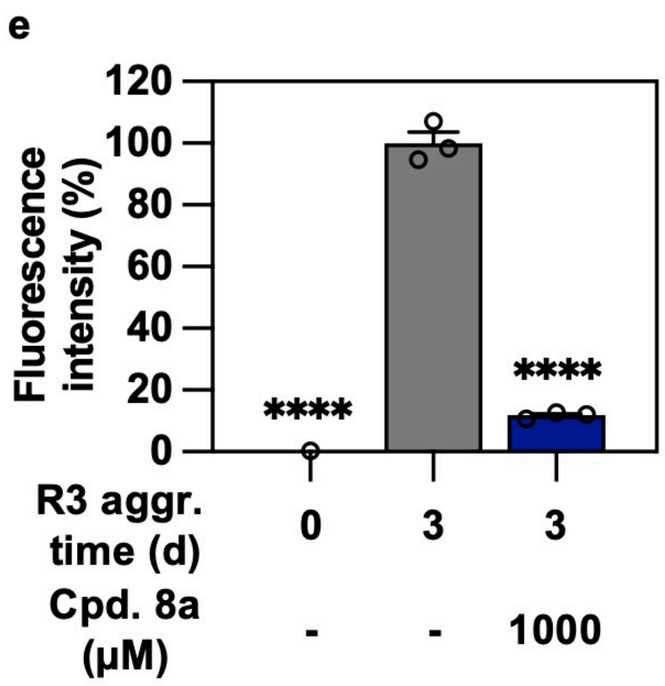
e
Fluorescence intensity (%)
120
100
80
60
40
20
0
****
****
R3 aggr. time (d)
0
3
3
Cpd. 8a (μM)
-
-
1000

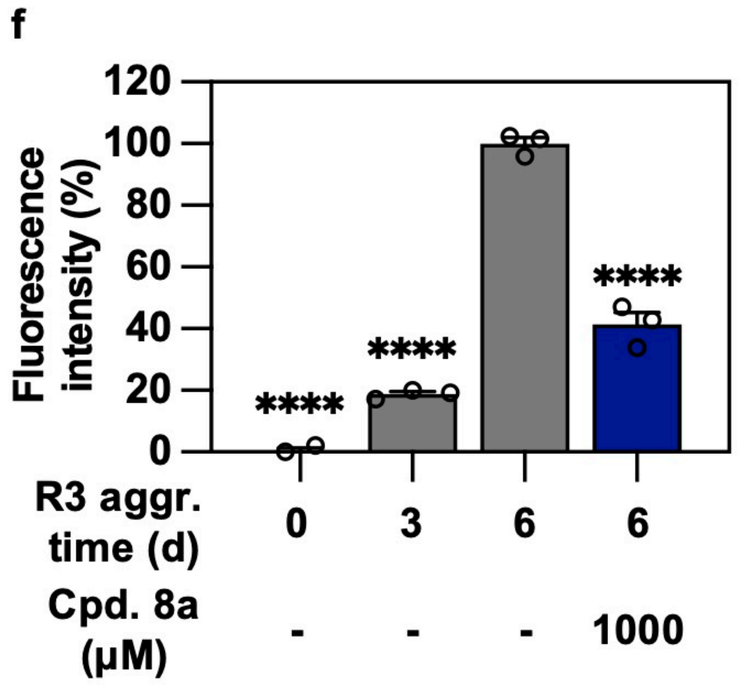
f
Fluorescence intensity (%)
120
100
80
60
40
20
0
****
****
****
R3 aggr. time (d)
0
3
6
6
Cpd. 8a (μM)
-
-
-
1000

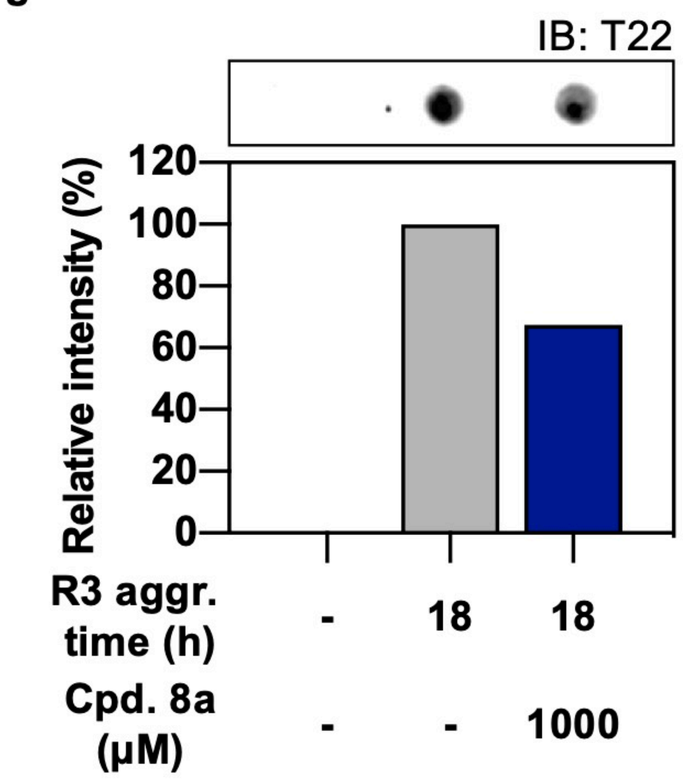
g
IB: T22
Relative intensity (%)
120
100
80
60
40
20
0
R3 aggr. time (h)
-
18
18
Cpd. 8a (μM)
-
-
1000

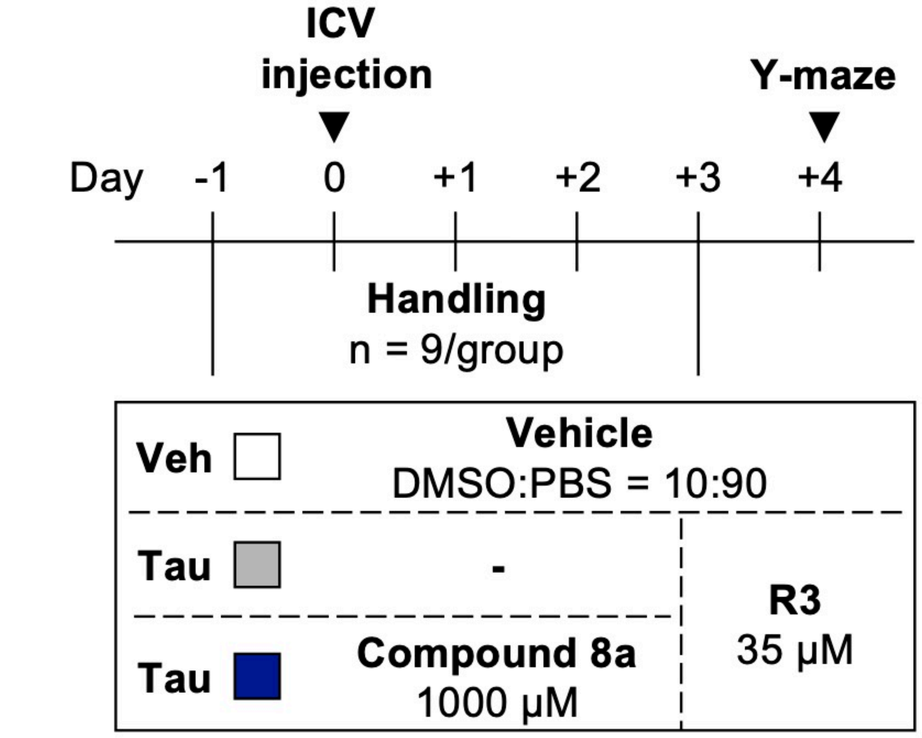
h
ICV injection
Y-maze
Day -1 0 +1 +2 +3 +4
Handling
n = 9/group
Veh
Vehicle
DMSO:PBS = 10:90
Tau
-
Tau
Compound 8a
1000 μM
R3
35 μM

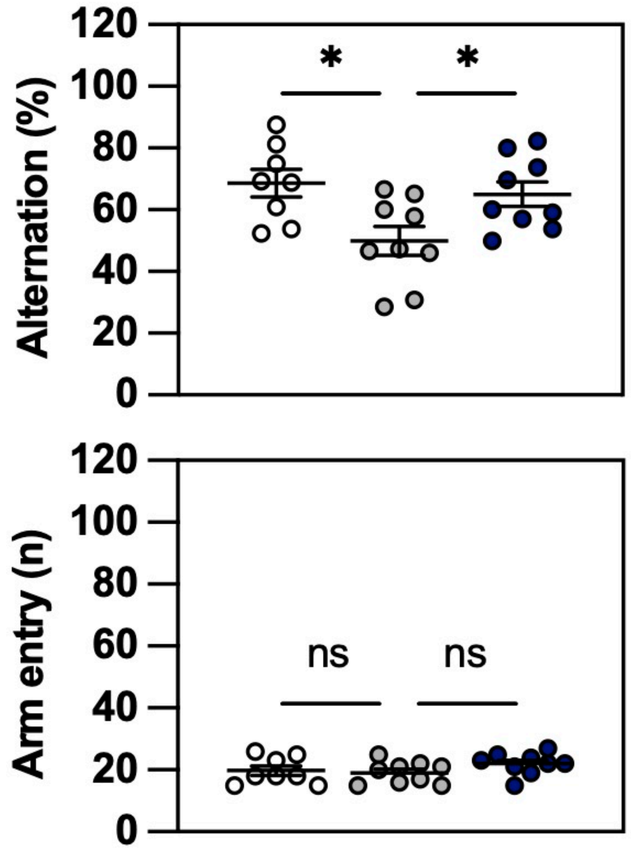
Alternation (%)
120
100
80
60
40
20
0
*
*
Arm entry (n)
120
100
80
60
40
20
0
ns
ns

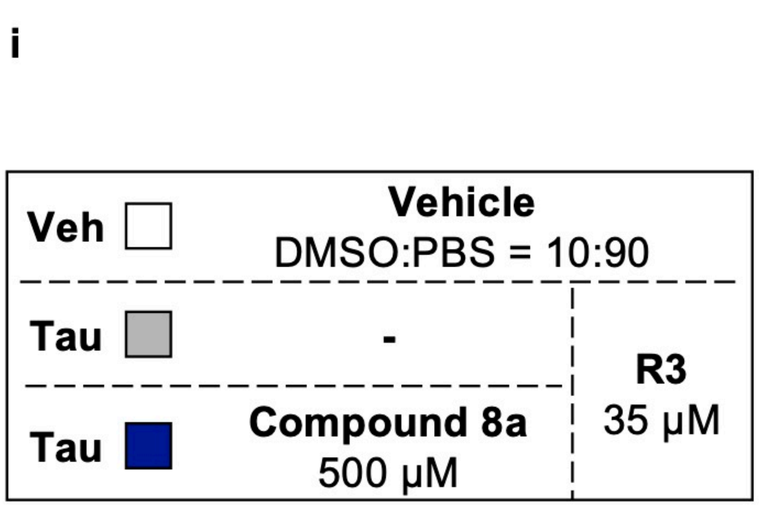
i
Veh
Vehicle
DMSO:PBS = 10:90
Tau
-
Tau
Compound 8a
500 μM
R3
35 μM

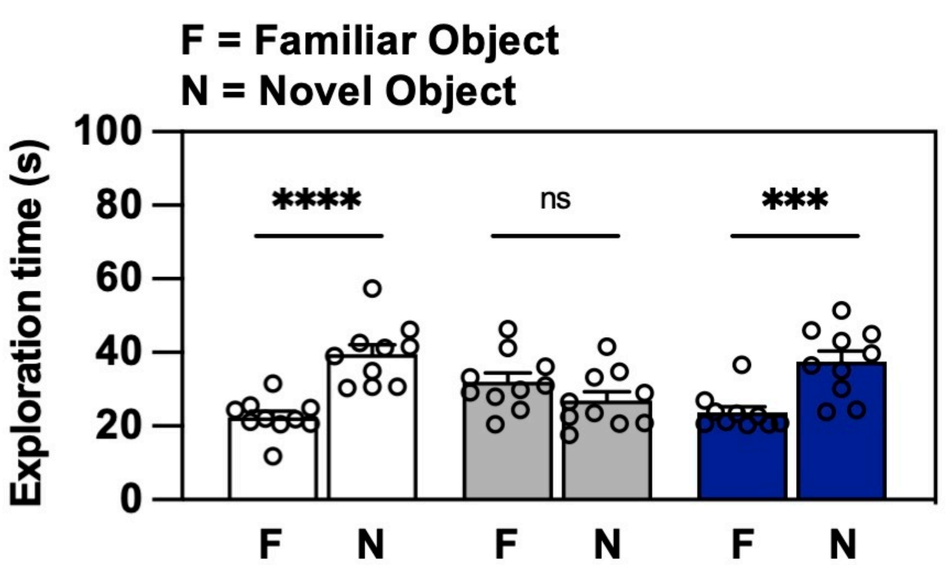
F = Familiar Object
N = Novel Object
Exploration time (s)
100
80
60
40
20
0
****
ns
***
F
N
F
N
F
N

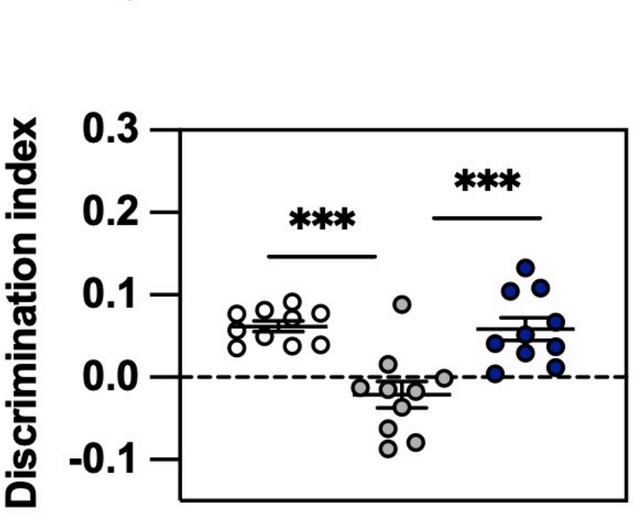
Discrimination index
0.3
0.2
0.1
0.0
-0.1
***
***